VSB - Technical University of Ostrava

Faculty of Mechanical Engineering

Department of Control Systems and Instrumentation

Srikanth Sreethar

Active Controlled Structure

Diploma thesis

Thesis supervisor:
Ing. Pavel Šuránek, Ph.D.

Ostrava 2021

ANNOTATION OF DIPLOMA THESIS

SREETHAR, S. Active controlled structure: Diploma Thesis. Ostrava: VSB-Technical University of Ostrava, Faculty of Mechanical Engineering, Department of Control Systems and Instrumentation. Thesis head: Šuránek, P.

The diploma thesis is focused to achieve vibration control of the structure. The experimental setup for the laboratory model is explained. The identification and approximation of the model was completed, the control algorithm was designed. The effectiveness and efficiency of the control algorithm is shown in graphical representation. The active vibration of the lattice tower structure would be helpful for the control of the lattice tower structures that induces vibration due to environmental effects and loads.

KEYWORDS

Active Vibration Control, Active control structure, Vibration control Methods, Vibration Control efficiency, Lattice structure.

ANOTACE DIPLOMOVÉ PRÁCE

SREETHAR, S. Aktivně řízená konstrukce: Diplomová práce. Ostrava: VŠB-Technická univerzita Ostrava, Fakulta strojní, Katedra automatizační techniky a řízení. Vedoucí práce: Šuránek, P.

Diplomová práce je zaměřena na téma řízení vibrací konstrukce laboratorního modelu. Je zde vysvětleno nastavení experimentu s laboratorním modelem. Byla dokončena identifikace a aproximace modelu a byl navržen algoritmus řízení. Účinnost a efektivita řídicího algoritmu je znázorněna graficky. Aktivní vibrace konstrukce příhradové věže mohou být užitečné pro řízení vibrací konstrukcí příhradových věží, které vyvolávají vibrace v důsledku vlivů a zatížení prostředí.

KLÍČOVÁ SLOVA

Aktivní řízení vibrací, aktivně řízená konstrukce, metody řízení vibrací, účinnost řízení vibrací, příhradová konstrukce.

TABLE OF CONTENTS

LIST OF FIGURES

LIST OF TABLES

LIST OF ABBREVIATIONS AND SYMBOLS

3D	Three dimensional	
AMD	Active mass damper	
AVC	Active vibration control	
CCLD	Constant current line drive	
CL	Constraining layer	
DAQ	Data acquisition module	
FEM	Finite element method	
FFT	Fast Fourier transform	
FLD	Free layer damping	
FRF	Frequency response function	
ISO	International organization for standardization	
PCLD	Passive constrained layer damping	
RMS	Root mean square	
SMA	Shape memory alloy	
TMD	Tuned mass damping	
TVD	Tuned viscous damping	
VEM	Viscoelastic material	
A	System gain	[m/V]
$a(t)$	Acceleration	[ms^{-2}]
f_r	Resonant frequency	[Hz; s^{-1}]
$G_{pe}(s)$	Transfer function (piezo - accelerometer)	[ms^{-2}/V]
$G_{sh}(s)$	Transfer function (shaker - accelerometer)	[ms^{-2}/V]
H_{max}	Maximum value of frequency response	[ms^{-2}/V]
s	Complex variable	[s^{-1}]
t	Time	[s]
$u_{pe}(t)$	Actuator voltage input	[V]
$u_{sh}(t)$	Shaker voltage input	[V]
ξ_o	Damping ratio	[-]
σ	Bandwidth for 0.707 max or -3dB	[Hz; s^{-1}]
ω_r	Resonant frequency	[rad s^{-1}]

1 INTRODUCTION

The main motive of this diploma thesis was to create a test structure that had to be excited with vibrations and create a control algorithm to control the vibrations using active vibration control. The structure here represents a lattice tower structure that uses mechanical components, the vibrations are excited to the structure from the dynamic shaker through Hiwin rails and the vibrations are controlled by the algorithm in which output is driving the voltage supplied to the piezo actuator.

Vibration is a mechanical phenomenon whereby oscillations occur about an equilibrium point. From (Takács, et al., 2012) we infer that undesirable mechanical and structural vibrations can cause discomfort in humans and certain engineering applications or can as well lead to catastrophic failure, structural failure, fatigue, splintering or other extreme consequences.

From (Rao, 2003) we infer that Vibrations are caused due to sudden disturbance for example due to environmental loads, induced self-excited elements, forces, non-linear responses and large deformations. Vibration are mechanical oscillations about an equilibrium position. There are cases in which vibrations are desirable, they are types of machine tools or production lines. However, in most of the cases the vibration of mechanical systems is undesirable as it wastes energy, reduces efficiency, may lead to wear and tear, may be harmful or dangerous as well.

The modern design shift towards lightweight materials such as aluminium and load carrying systems utilizing cables has contributed to important advances in the design and construction of visually pleasing structures. These structures have an exclusive design process focused on ease of constructability and minimizing material usage. Though both these result in very efficient design, the reduces self-weight include a reduction in the structure inherent damping and lower natural frequencies. This increases the dynamics sensitivity which results in structure that are prone to excessive vibrations and often requires vibration control and vibration mitigation strategies in order to satisfy the required service life span.

From (Rahman, 2015) all the types of vibration control approaches are categorised into the three types which are passive vibration control, active vibration control, semi-active vibration control. To eliminate or reduce and control the reaction towards vibrations we use active vibration control and active vibration-controlled structures.

One can classify the mechanical vibrations acting according into two types based on whether an outside force is exciting the vibration that is free vibration and forced vibration. In free vibration the mechanical system is excited by an initial condition such as displacement or velocity and then can vibrate freely without further force interactions. Forced vibration is when an alternating force or motion is applied to mechanical system. Forced vibration is a type of vibration in which a force is repeatedly applied to a mechanical system.

The types of vibration control approaches are inferred from (Kandasamy, et al., 2016). They are passive vibration control, active vibration control, Semi active vibration control and hybrid vibration control. The vibration control system is called passive if it uses passive device in which it does not require an external power source for its operation and utilizes the motion of the structure to develop the control forces. It usually consists of viscoelastic damping layers. A vibration control system is called active if it uses external power to perform its function Active methods generate control forces on the structure to control vibrations. It is Usually based on a feedback system of sensors and actuators. The semi-active vibration control system requires typically a small external power source for its operation and utilizes the motion of the structure to develop control force, where the magnitude of the force can be adjusted by an external power source accordingly. It uses the advantages of both active and passive devices. Semi-active systems or tuneable passive systems control some tuneable parameter (example - stiffness or damping) to achieve vibration control. Examples include shape memory alloys, pneumatically controlled granules, electro/magneto-rheological fluids. Hybrid methods combine robustness of the passive device and high performance of the active devices. This has resulted in enhanced vibration suppression over a wider frequency and excitation range and has overcome some of the drawbacks of active or passive alone treatments.

This document consists of chapters with different sections. The second chapter consists of design of components of the laboratory model such as bottom plate, upper plate, connecter, linear guide rails, linear guide block, the assembly design and drafts of the components designed and the assembly draft. The third chapter consists of experimental realisation of the designed components and the connection between them and pictures of the working laboratory model. In the experimental realisation the completed structure, power amplifier and its specification, the generator and its specification, piezo amplifier, electrodynamic shaker, piezo accelerometer, piezoelectric actuator. The fourth chapter contains the measurements taken to identify the system. In this chapter the different measurements such as frequency response function and the plots of the measure are inserted. Then further identification of the system is done to identify the system

behaviour if its proportional, derivative or else integral in nature. The major parameters to perform the identification experiment are the knowledge of Hanning window, Auto spectrum, Frequency response function.

Then the design of the control algorithm was done using Simulink tool in MATLAB, which is explained, the same control strategy was designed in dSpace to perform the AVC on the laboratory model and the results were obtained and the data was analysed.

The efficiency and effectiveness of the AVC is explained in the last chapter which shows the AVC having good efficiency, which can be inferred from the results obtained and the respective plots are plotted.

2 STATE OF ART IN VIBRATION CONTROL AND SMART MATERIALS

The various methods of vibration control are passive methods, active methods, semi-active methods which further have different categories which are explained in detail in this section. Then the smart materials used in active vibration control are explained.

2.1 PASSIVE METHODS

From (Kandasamy, et al., 2016) passive methods are categorised by the structural addition of typically viscoelastic damping layers, where the hysteresis loop of the cyclic stress and strain of the damping layer dissipates vibration energy. There are three main methods of passive vibration control, namely free-layer damping treatment (FLD), constrained-layer (PCLD) or sandwich-layer damping treatment and tuned viscoelastic damper (TVD).

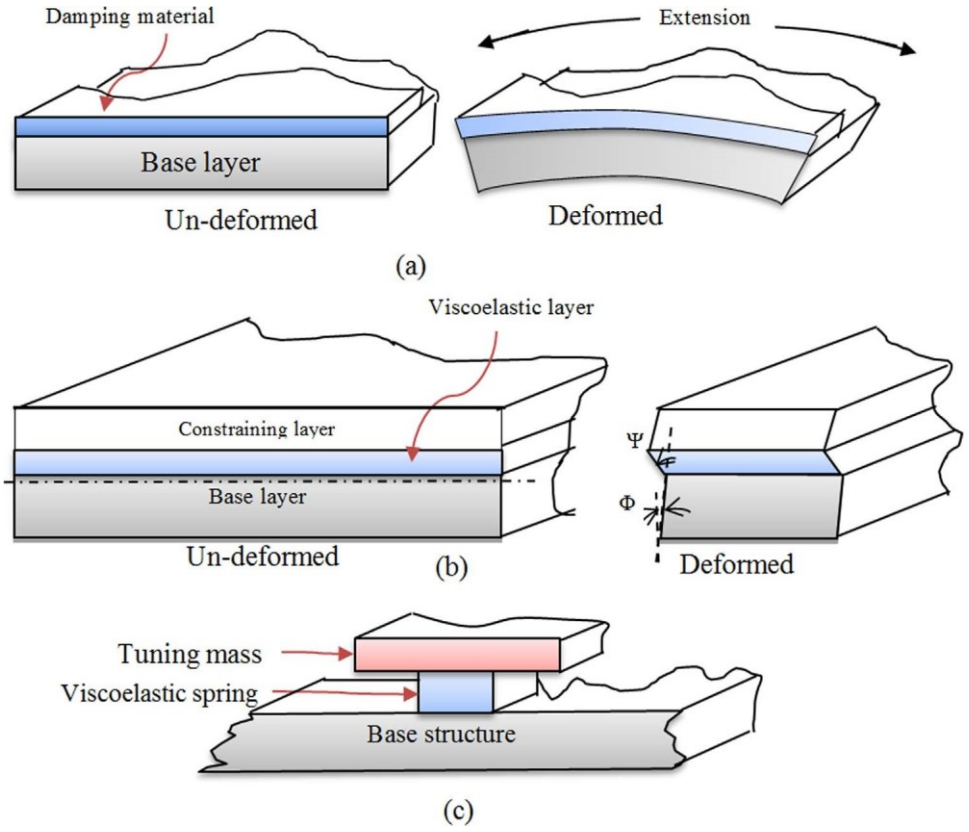

Figure 2.1 Passive vibration control methods [(a) free-layer damping treatment (FLD) *(Kandasamy, et al., 2016)***, (b) passive constrained layer damping (PCLD)** *(Uppal, 1996)***, (c) tuned viscoelastic damper (TVD)** *(Rao, 2003)***]**

Free-layer damping treatment (FLD) which is also called as extensional type damping treatment where the damping material is fused using an adhesive on the structure. The viscoelastic material

deforms mainly in planes parallel to the base structure when the base structure is bent in bending. The hysteresis loop of the cyclic stress and strain dissipates the energy (vibration).

Passive constrained layer damping consists (PCLD) of three layers they are a base structure layer, a viscoelastic material (VEM) layer, and a constraining layer (CL). As the base layer is subject to bending (vibration), shear deformation of the VEM layer occurs, dissipating energy.

Tuned mass damper (TMD) consists of mass on linear spring which has the natural frequency the same as the natural frequency of damped system. Tuned viscoelastic dampers (TVDs), which make use of viscoelastic polymers are modelled as simple masses assigned to viscoelastic spring elements (damping polymers). TVDs are useful for vibration reduction of a (known) single frequency or narrow band of frequencies. Correctly tuned TVDs can remove unnecessary resonance by splitting the original peak into two, one below and one above the resonance frequency of the original system.

2.2 ACTIVE METHODS

An active control typically requires power source for the operation of electrohydraulic or electromechanical (servo motor) actuator, which provides better structural damping or stiffness. In general, active damping is achieved either by open loop or feedback or feed-forward with aid of pairs of lumped sensors and actuators. When the piezoelectric actuators and sensors, being stimulated with proper control effort, are either attached on or inserted into the base structures, the resulting structures achieve self-sensing and self-controlling capabilities. Active methods able to adapt to environmental changes and potentially perform self-diagnosis inferred from (Korkmaz, 2011).

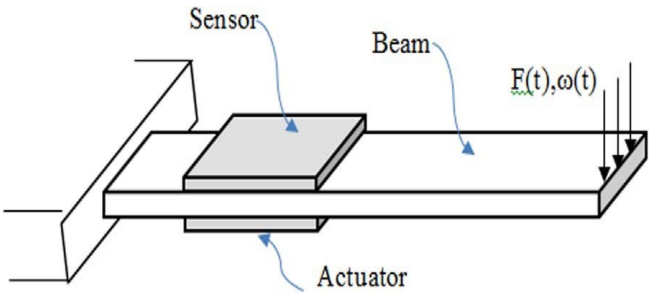

Figure 2.2 Cantilever smart piezoelectric beam *(Vasques, 2006)*

Piezo active damping consists of Piezoelectric materials are capable of transducing mechanical to electrical energy and vice versa. When these materials are subjected to an electric field, produce a mechanical strain, generate electricity under the action of mechanical strain. These effects (direct

and converse piezoelectric) have enabled piezoelectric materials to perform as sensors and actuators in vibration control applications. A typical active vibration control of a cantilever aluminium beam with pair of collocated piezoelectric patches mounted on the surface.

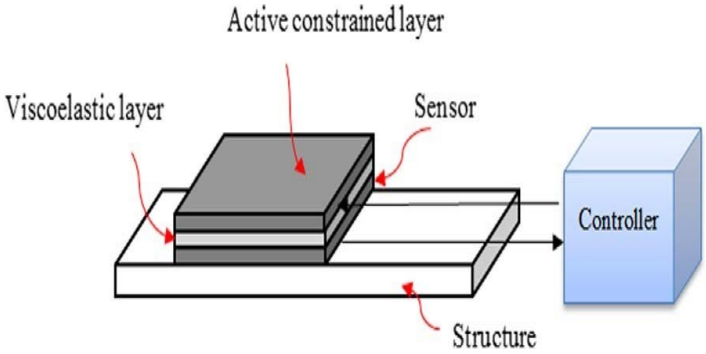

Figure 2.3 Schematic of active constrained layer damping *(Ng, 1997)*

Active constrained layer damping is basically a viscoelastic damping layer inserted between two piezoelectric layers, where the piezoelectric layers sense and control the shear of the viscoelastic layer to provide vibration control. One piezoelectric layer, directly linked to the structure, acts as a sensor (with supply voltage V_s). The other piezoelectric layer acts as an active constrained layer, activated by the control voltage V_c.

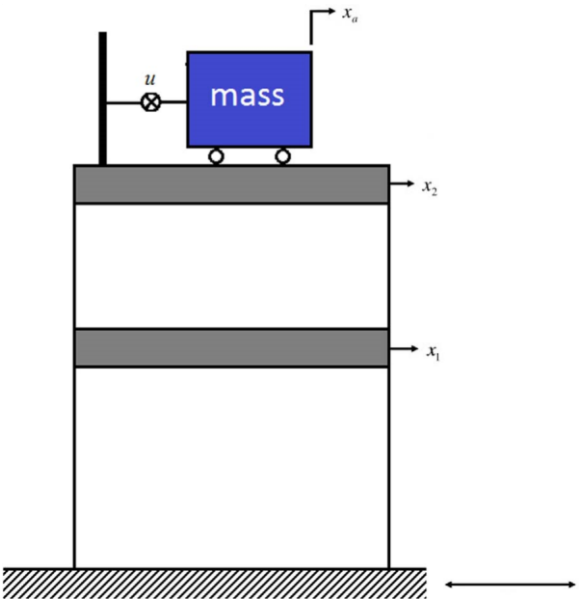

Figure 2.4 Schematic representation of AMD technique *(Ricciardelli, 2003)*

The active form of the mass damper is the active mass damper, in which the mass is associated to the structure through an actuator and sensor. AMDs have been used to reduce the structural vibrations of structures under strong winds and mild earthquake.

2.3 SEMI-ACTIVE METHODS

Semi-active control methods modify or control the mechanical properties of the damping element within the vibration control device. This usually requires a small amount of external power for operation (on the order of tens of watts). Examples of semi-active control methods include shape memory alloys and pneumatically controlled granules inferred from (Kandasamy, et al., 2016).

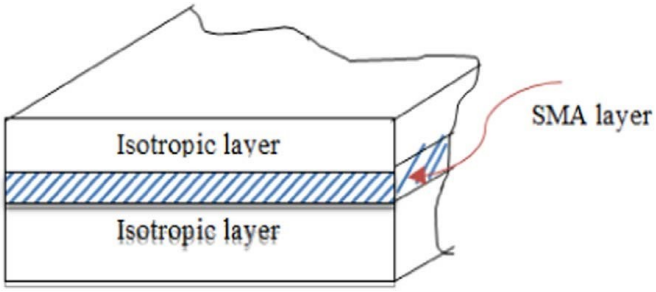

Figure 2.5 SMA laminated composite *(Damanpack, 2014)*

Shape memory alloys (SMA) can be rooted into a structure and used to control the shape, structural modes and reduce vibrations. SMAs can be realized as passive damping or semi-active damping elements.

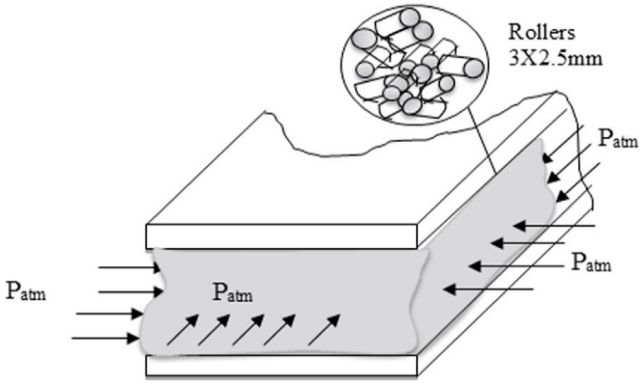

Figure 2.6 Pneumatically controlled granular structure *(Bajkowski, 2016)*

Pneumatically controlled granular structures are small loose, elastic grains or rollers (example - 2 mm) silicone rollers held airtight between two layers. The granular structure maintains continuous contact to the elastic layer and exhibits a reversible phase transition of the material from a fluid-like to semisolid state under or by varying the pressure among the granules. During deformation of the granular structure, the particle movement causes the dissipation of energy through non-conservative interactions, which bring together friction, slips, particle hopping or intrusion, local deformations, etc. The level of energy dissipation depends primarily on the state of the granular matter.

2.4 SMART MATERIALS IN ACTIVE CONTROL VIBRATION

Feedback control system must have important components like the hardware computing control unit input through the strategy of our choice, include sensors to provide feedback to the controller and the actuators to carry out the changes required in the plant dynamics.

There are traditional actuating components like electromagnetic devices, pneumatic actuators, rotary and linear motors. They are effectively utilized in vibration control. Modern engineering material referred to as intelligent or smart have the advantage of being light also which are structurally integrated. The most common smart materials used in active vibration-controlled structures are shape memory alloys, magneto as well as electro strictive materials, semi-smart magneto and electro-rheological fluids where the coupling is one directional, electro chemical materials and piezoelectric. The smart materials in active vibration control are inferred from (Takács, et al., 2012) and (Takács, et al., 2014).

Shape memory alloys (SMA) reveal apparent plastic deformation and recovery to the original shape after heating. SMA can recover as much as 5% strain compared to materials like piezoceramics is a considerable change. The shape change might be due to temperature changes which results in solid state phase deformation. This deformation is called martensitic deformation. The common materials used for SMA are nitinol, nickel and titanium-based alloys, copper-based alloy.

Figure 2.7 SMA materials can be memorized to different shapes. The wire and the plates on the left are set to a straight shape, while the darker plate is memorized to a curved shape *(Takács, et al., 2012)*

The major properties that the SMA present are super elasticity and shape memory effect. super elasticity is the ability of the material to return to its original shape after a considerable amount of mechanical stress and deformation. Shape memory effect is the property of the SMA to return to its original shape after applying a small amount of heat.

The SMA are used in both active and passive vibration control and the behaviour are studied using analytic and FEM methods.

Magneto-strictive and Electro-strictive materials demonstrate the shape change upon the application of magnetic and electric fields. Magneto-strictive (MS) materials change their shape when imperilled to the magnetic field. All the ferromagnetic materials demonstrate this property, but the shape and volume change are small.

The deformation in magneto-strictive materials is characterized with the magneto-strictive coefficient, which expresses the fractional length change upon applying a magnetic field. The shape change of the material is zero at zero magnetic field, however upon the application of the field it grows linearly according to the magneto-strictive coefficient until the material reaches magneto-strictive saturation.

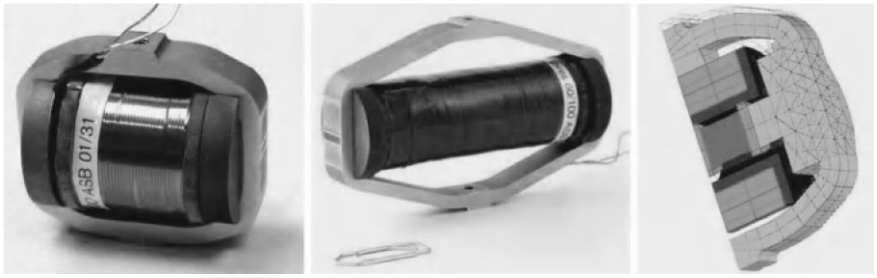

Figure 2.8 Prototypes of different magneto-strictive actuators *(Takács, et al., 2012)*

The electro-strictive materials are dielectrics. Dielectrics change their shape upon the application of an electric field. If the material is subjected to a strong electric field, the opposing sides of these fields become charged with a different polarity. All dielectrics exhibit some level of electrostriction. A class of engineering ceramics does produce greater strains than other materials. Such materials are known as relaxer ferroelectrics.

Fluids based on the magnetorheological (MR) and electrorheological (ER) effects include suspended particles, which upon the application of a magnetic/electric field align themselves to form columns within the fluid.

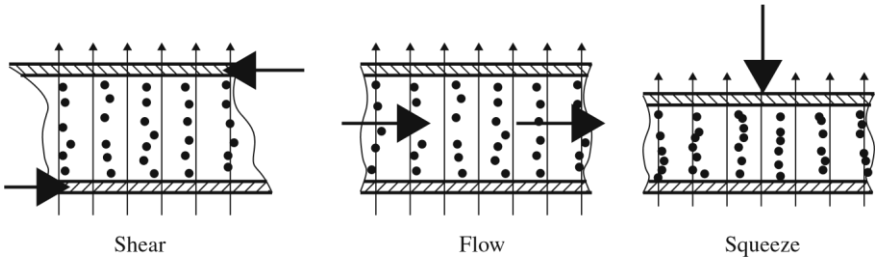

Figure 2.9 Different operation modes for an MR fluid-based damping device. Thick arrows denote movement directions, while thin arrows represent magnetic flux lines *(Takács, et al., 2012)*

The columns of suspended particles create hurdle for fluid flow, thus boosting the overall net viscosity of the system. Damping systems using MR or ER fluids cannot supply energy to the controlled system, may change the damping properties according to a controller strategy.

In shear mode, one plate is moving in relation with each the other in a direction perpendicular to the magnetic flux and the particle columns. In flow mode, the plates are stationary, the fluid is moving due to a pressure difference. In the squeeze-flow mode, the plates are moving in relation to each other, however this time the movement is carried out along the flux lines and the particle columns.

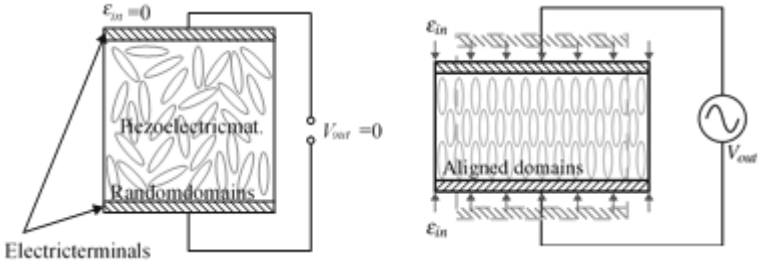

Figure 2.10 The direct piezoelectric effect, or in other words the piezoelectric material in sensor mode *(Takács, et al., 2014)*

Piezoelectricity is the ability of certain materials to generate an electric charge in response to an applied stress inferred from (Takács, et al., 2014).

If the material is not short-circuited, the charge induces a voltage. This is the so called direct piezoelectric effect. The piezoelectric effect is reversible, meaning that applied voltage generates mechanical stress and deformation. This is known as the converse piezoelectric effect.

3 DESIGN OF COMPONENTS AND EXPERIMENTAL SETUP

In this chapter the design of varies components used for the experimental setup is explained in detail and the roles of the respective parts or components are explained.

3.1 BOTTOM PLATE

The bottom plate is the plate that is placed above the table present in the laboratory and are fixed to the table using the fasteners like bolts and nuts. The material used for the bottom plate is Aluminium Al5083 which is an Aluminium alloy with Magnesium and traces of Manganese and Chromium and the material properties were applied to the bottom plate using the Creo software and the mass is calculated to be 8.39 kg.

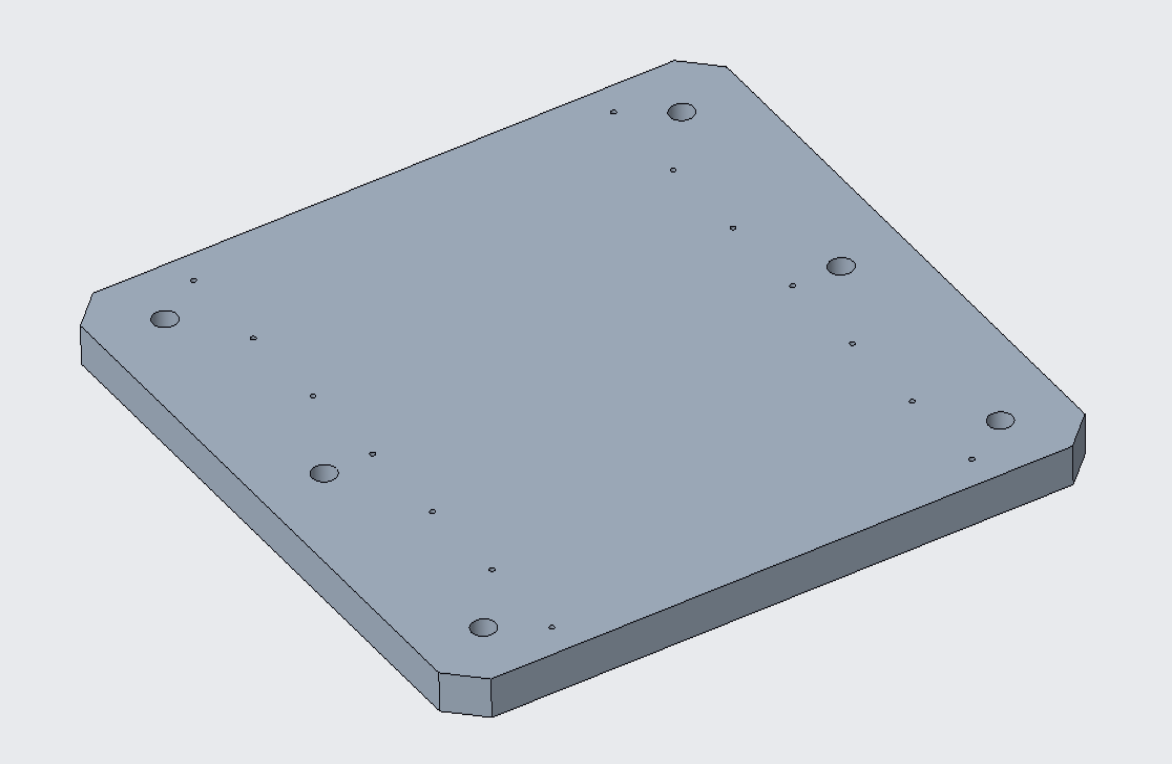

Figure 3.1 Bottom plate part design screenshot from the Creo Parametric

The drafting of the component was done in order to get the designed component manufactured. The draft of the component provides the manufacturer with the dimensions of component, the tolerance and accuracy details.

The component requires enough strength as the position of the holes need to be accurate as the component houses the liner guide rails on top and the rest of the assembly on top. The major dimension of the bottom plate designed are 400 × 400 mm and thickness of 20 mm.

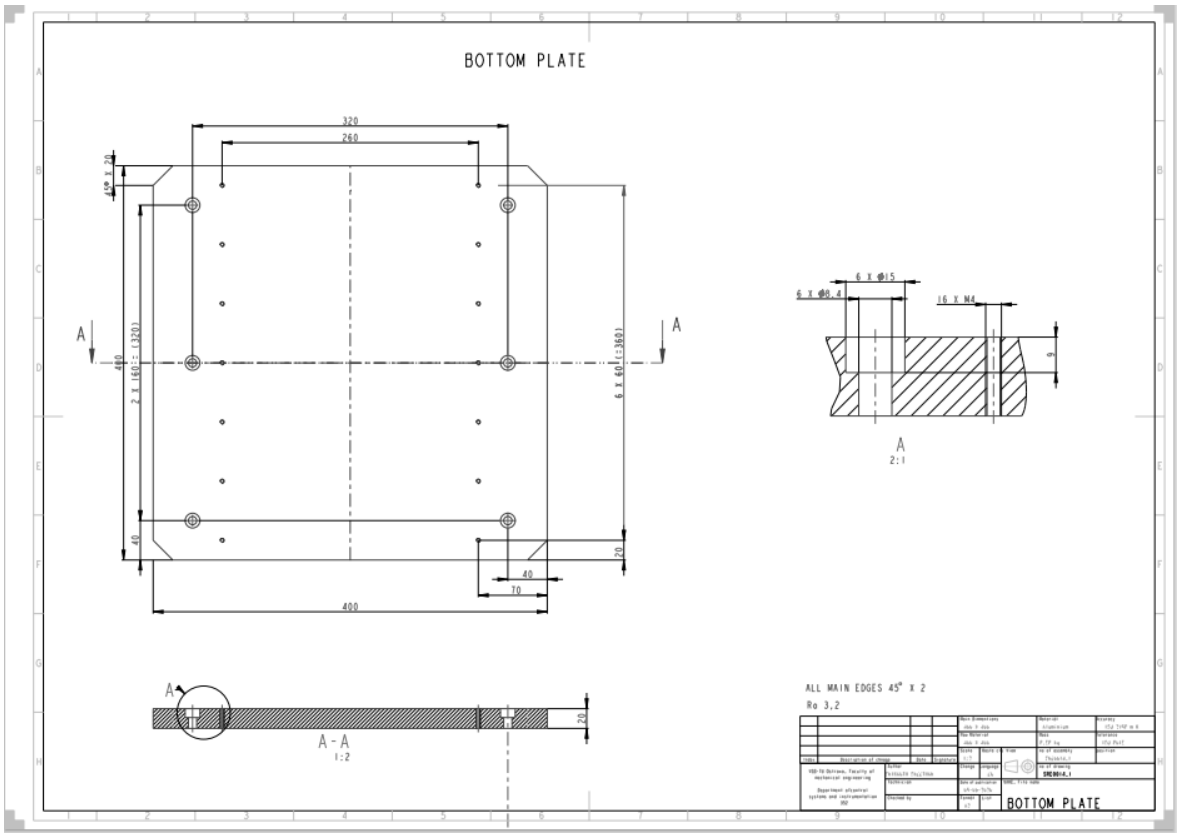

Figure 3.2 Draft of bottom plate

3.2 UPPER PLATE

The upper plate is the plate that is placed above the linear guide rail and are fixed to the liner guiderail using the fasteners like bolts and nuts. The material used for the upper plate is Aluminium Al5083 which is having Poisson's ratio 0.33 and density of 2650 kgm^{-3} and the material properties were applied to the upper plate using the Creo software and the mass is calculated to be 6.29 kg.

The draft of the component is provided below which shows the dimensions and specification of the component. The draft of the component provides the manufacturer with the dimensions of component, the tolerance and accuracy details.

The component requires enough strength as the position of the holes need to be accurate as the component houses the structure attached with sensors and actuators and withstands the vibration the is excited from the vibration exciter which is the input of disturbance to the system.

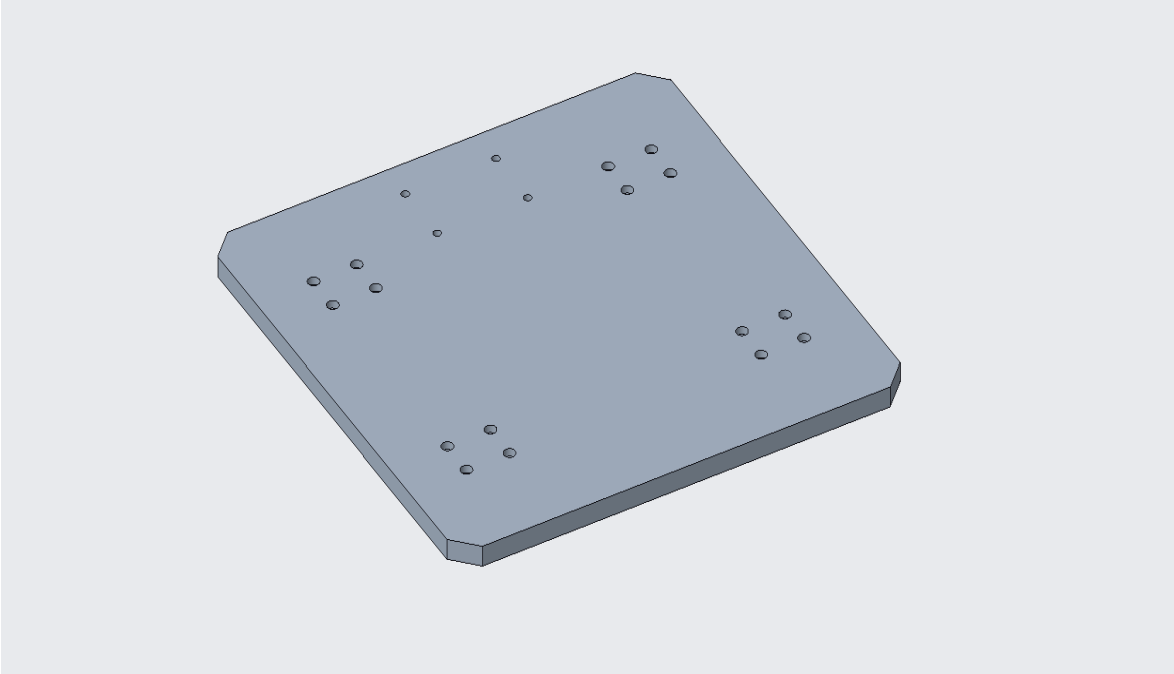

Figure 3.3 Upper plate part design screenshot from the Creo parametric

The major dimension of the upper plate designed are again 400 × 400 mm but having thickness of 15 mm.

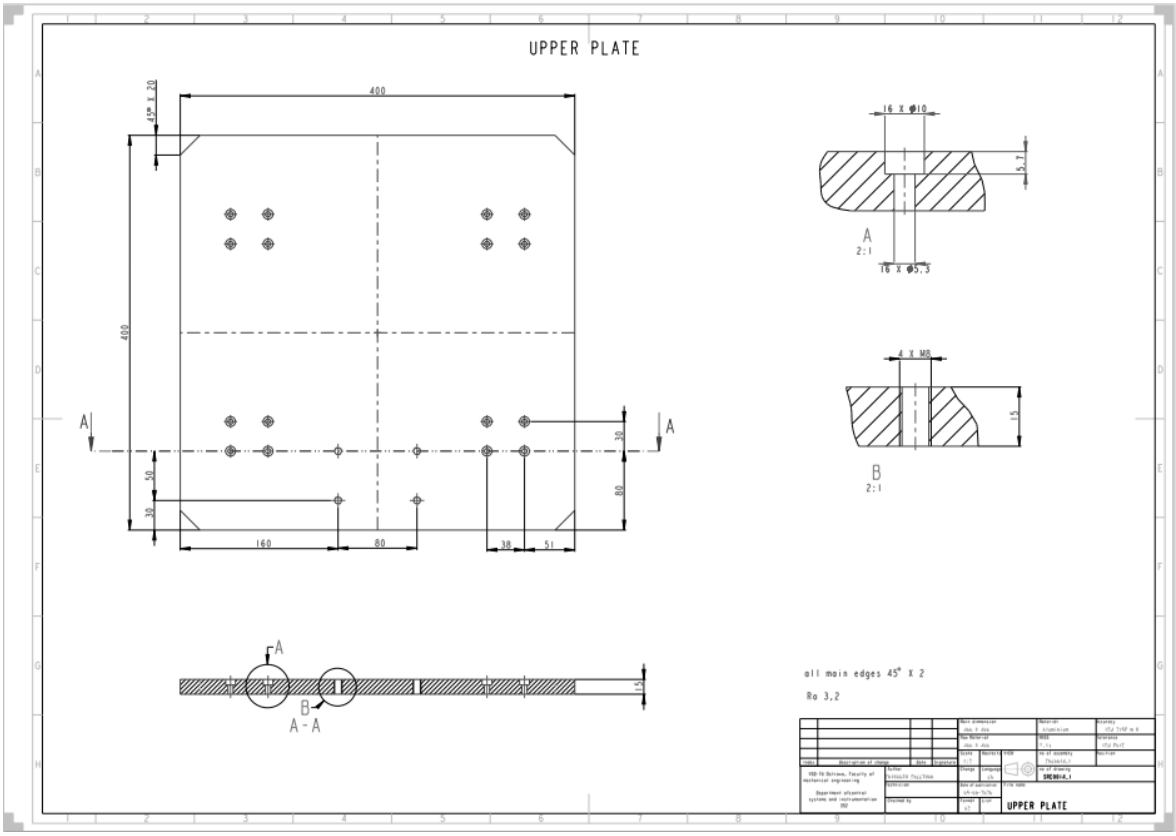

Figure 3.4 Design draft of upper plate

3.3 CONNECTER

The connecter is the part which is designed to connect the upper plate to the vibration exciter. This component was manufactured using 3D printing and the strength of material was sufficient and does move along with the vibration exciter arm to generate vibration on the plate which is transmitted to the structure.

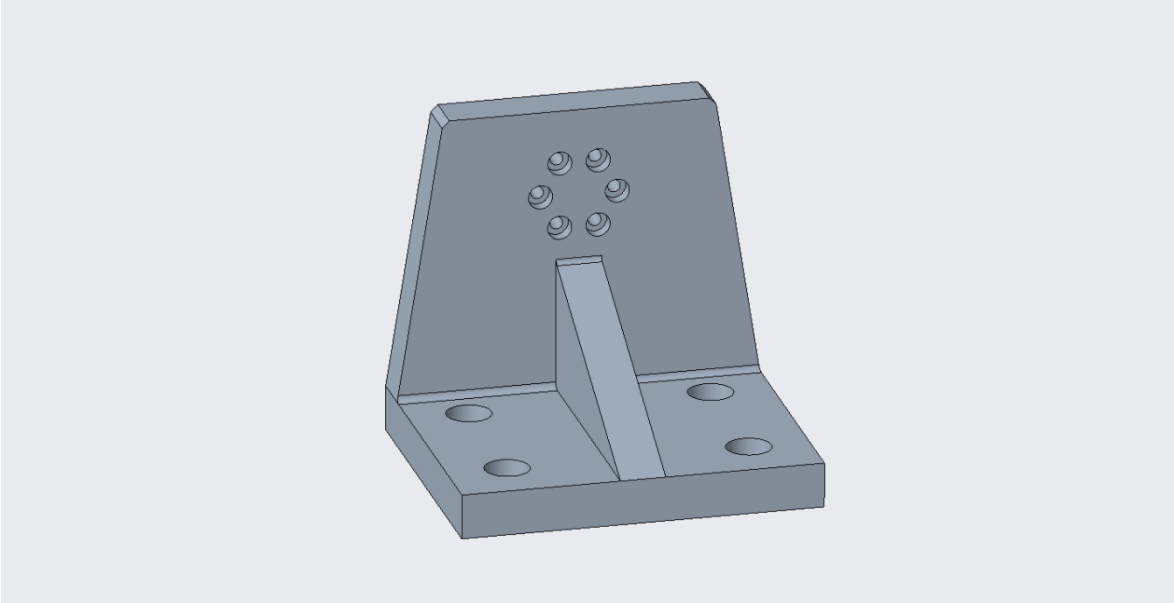

Figure 3.5 Connecter design screen shot from Creo parametric

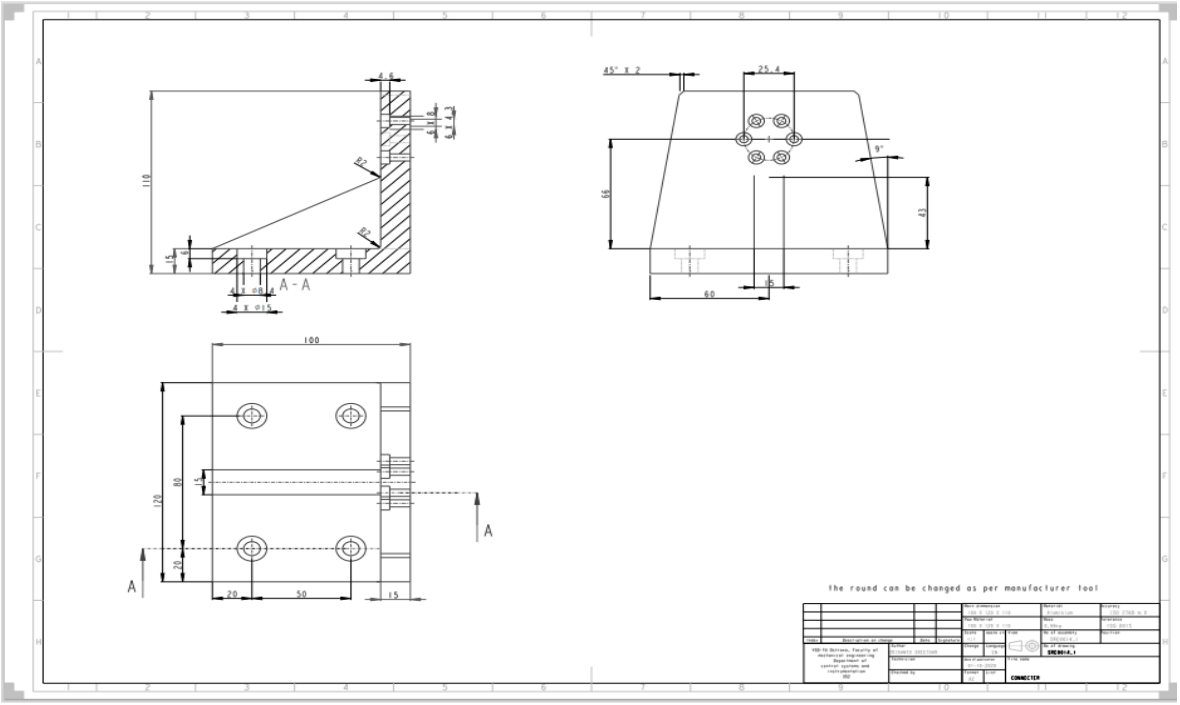

Figure 3.6 Design draft of connecter part

3.4 LINEAR GUIDE RAILS

The linear guide rails were brought from HIWIN s.r.o Czech Republic and the size selected based on the table size and the movement of rail blocks required. The linear guide rail was selected from the HGR15 series. The design of parts was downloaded from the HIWIN s.r.o official website as the parts were procured and were not drafted and manufactured. The part download for design was used as a reference model for the assembly.

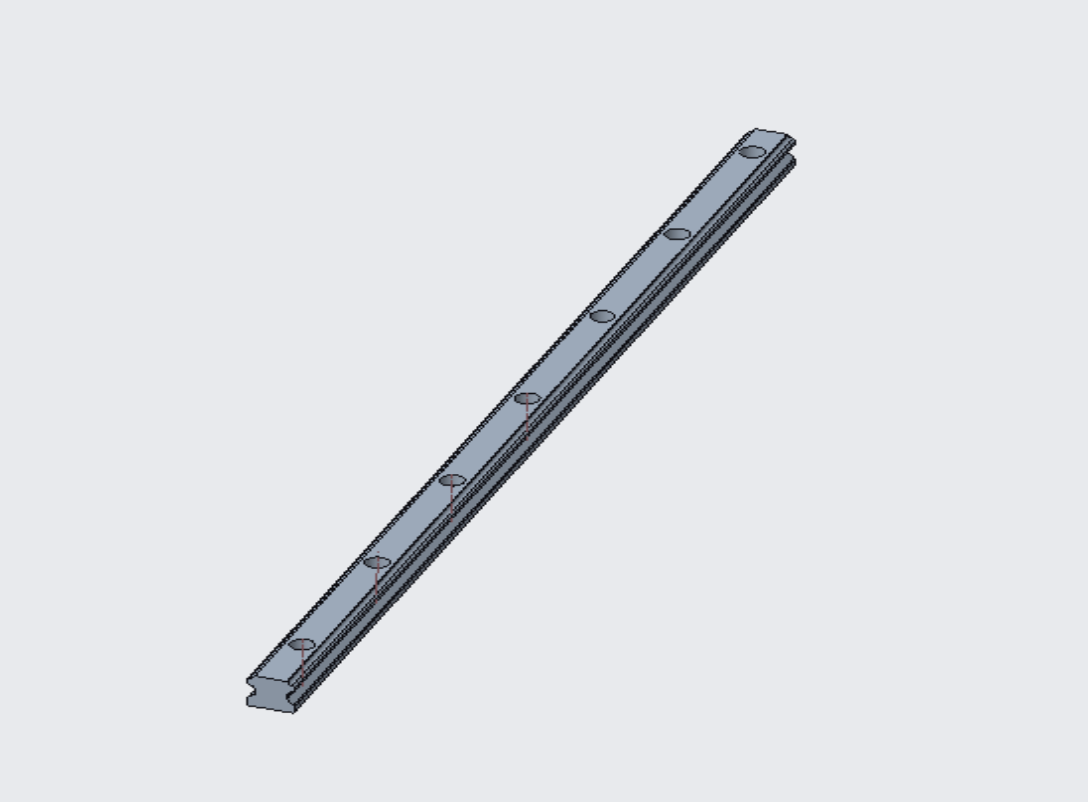

Figure 3.7 Design of linear rail procured from HIWIN s.r.o

The advantages of using the linear guide rail are it provides high positioning accuracy, long lifetime and highly precise movements, they require low driving forces, they can with stand high loads in all the directions.

The installation for the experimental setup is easier as it requires mechanical fasteners to fasten. The lubrication selected was minimal as they load is comparatively low and is used for working in a closed environment. It also is corrosive resistant and the wear due to movement is very low as it is sufficient lubricated, they are coated with the CTS or zinc material.

The product code of the linear rail is HGW15CC2R400Z0C2.

3.5 LINEAR GUIDE BLOCK

The linear guide block is used to take the load of the upper plate designed and the load of the structure. It balances the load; The movement of the upper plate is transmitted to movement of rail. The product was procured from the Hiwin s.r.o Czech Republic and the design file was downloaded for the reference purpose to design the remaining parts required for the assembly. The product code of linear rail block is HGW45 and is represented by the series HG15.

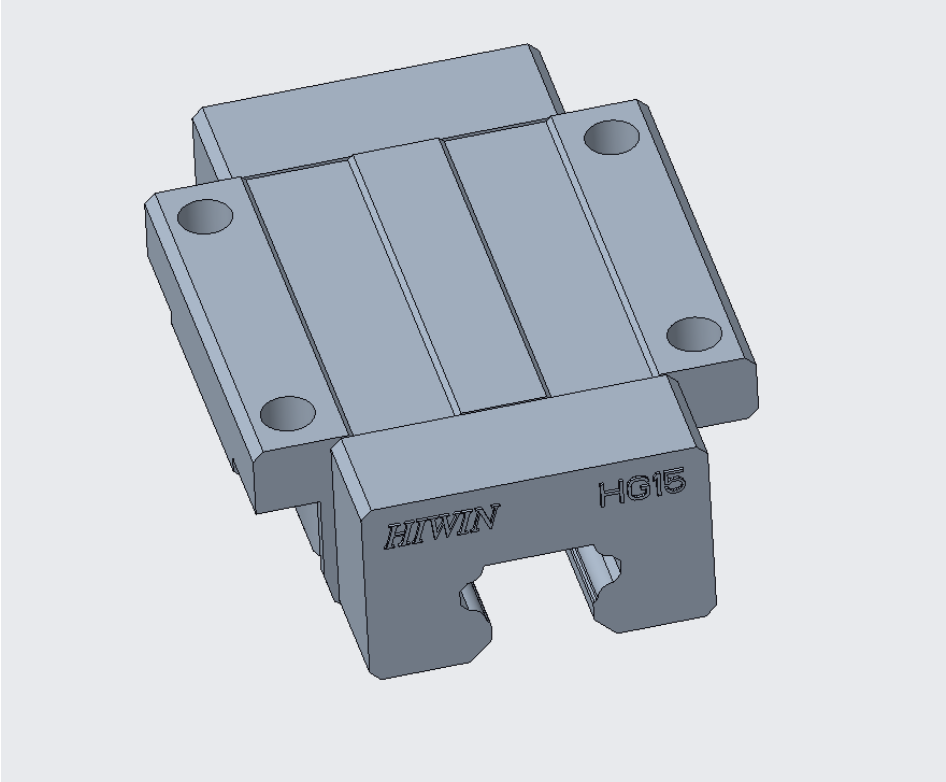

Figure 3.8 Design of Linear guide rail block procured from Hiwin s.r.o

The block used is of flange type. They are fastened to the linear rail from above. They have good dynamic moment, static moment, dynamic and static load rating.

3.6 ASSEMBLY DESIGN

The assembly design consists of the table design, bottom plate, upper plate, linear guide rail, linear guide block and the connecter. The screws used to fasten used are of ISO4762 of various sizes were used. The assembly of the designed components are shown in the below Figure 3.9 and the vibration exciter and the structure are not shown in this as the exciter used it to represent the external disturbance and the structure used is assembled in symmetrical shape and were from the Merkur blocks.

The assembly and the assembly draft are shown below so show the assembly of components for the representation purpose and the list of materials are shown in the assembly draft.

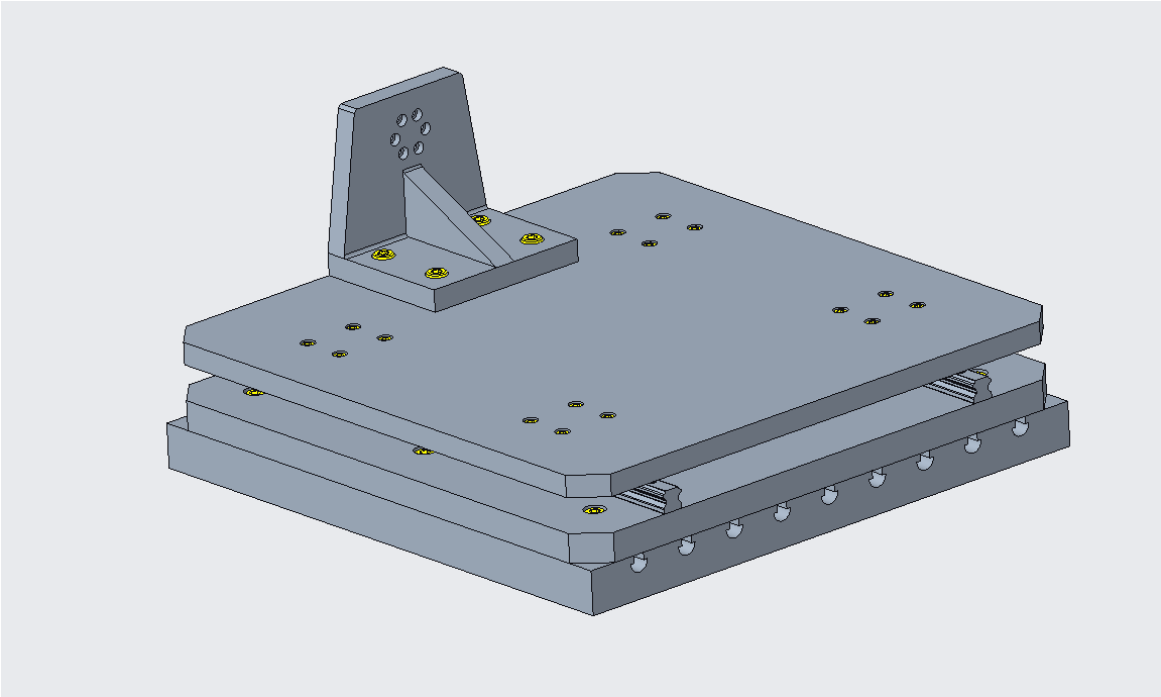

Figure 3.9 Assembly of the components used for experimental setup in Creo parametric

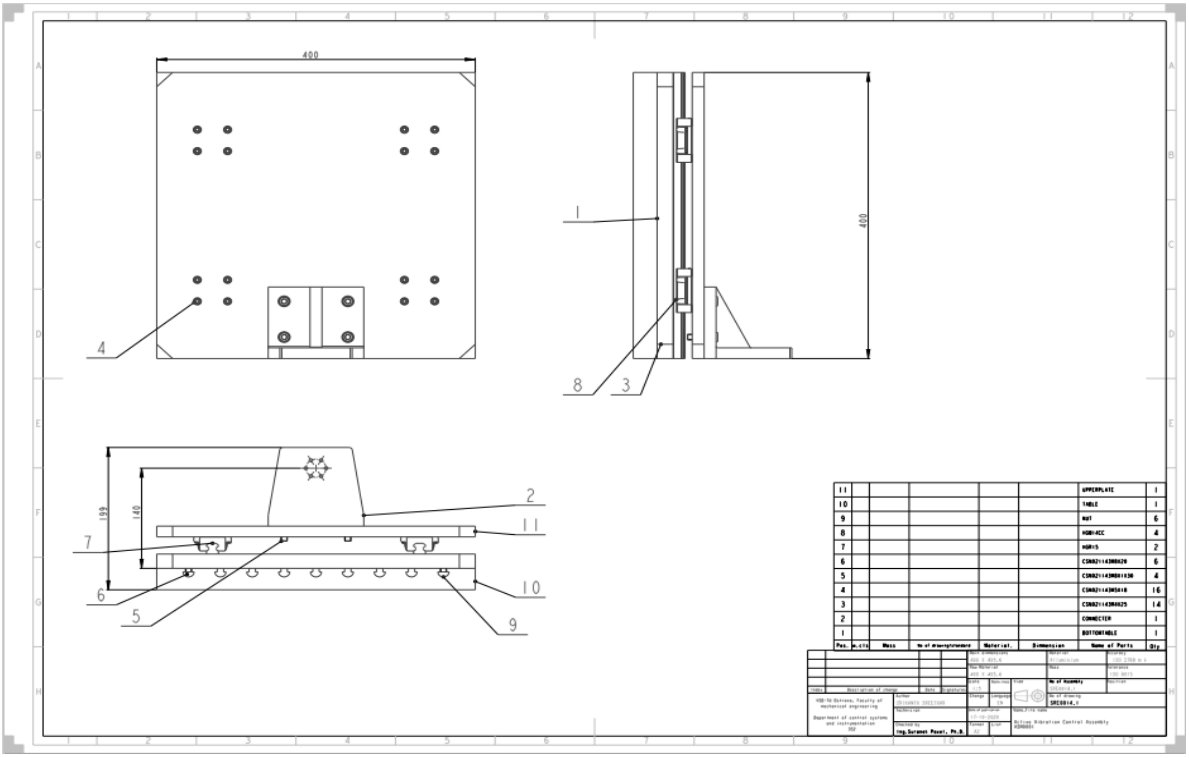

Figure 3.10 Assembly draft for experimental setup of Active-controlled structure

The assembly setup and the image of the respective components assembled for the experimental setup to perform the experiment and measure the required data are given.

3.7 STRUCTURE

The model selected is lattice tower structure which represents as a prototype to the tower or hive structure with mast. In first stage of modelling the lattice tower is being built using MERKUR materials. The four-sided symmetrical structure is being constructed and linkages are being fastened using mechanical fastener like nuts and bolt arrangement. Active vibration control will be executed on this structure.

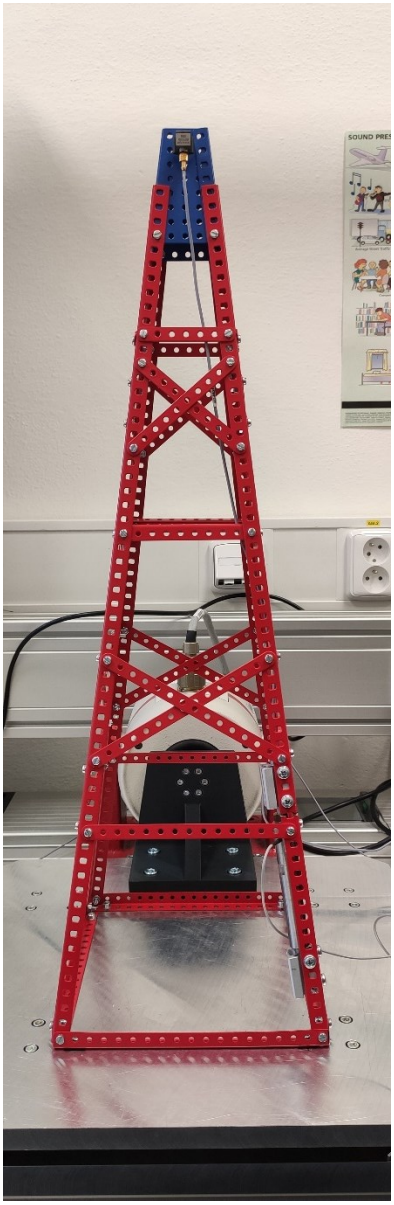

Figure 3.11 Lattice tower Structure built to perform active vibration control

The structure consists of upper cross members, main members, horizontal members and lower cross members. The top portion of the structure is called as mast. The lattice tower structure also represents structures like Eiffel tower in Paris and lookout tower in Prague.

3.8 POWER AMPLIFIER

The power amplifier is an electronic amplifier, the purpose of which is to increase the magnitude of power of the given input signal. The power of input signal is increased enough to drive the vibration exciter. The power amplifier used is LDS PA25E-CE which is designed to drive the electrodynamic shaker systems which is used to excite vibrations. The supply voltages are 230 V for frequencies 50 Hz.

Figure 3.12 Power amplifier LDS PA25E-CE

This power amplifier is connected from the power source to the electrodynamic shaker which is used to excite the vibrations that act as an external disturbance for the structure.

3.9 DATA ACQUISITION

The data acquisition module used is Bruel and Kjaer type 3160-A-042 which works as a standalone analyser test system which consists of four input ports and two output ports. The combination of input and output ports makes it versatile data acquisition module. The device works at a maximum frequency of 51.2 Hz. It converts the DC voltage to 51.2 kHz input range.

Figure 3.13 Bruel and Kjaer output generator Module Type 3160-A-042

The data acquisition module is connected to the Shaker and the accelerometer. The output from acquisition module data is accessed from the signal generator software from the laptop or computer device. The first output channel is used for to manage excitation and the second channel is used to measure. The first input channel measures the excitation signal.

3.10 PIEZO POWER AMPLIFIER

The PI LVPZT amplifier is used to amplify the signal for piezo actuator. It supports operation of up to three channels.

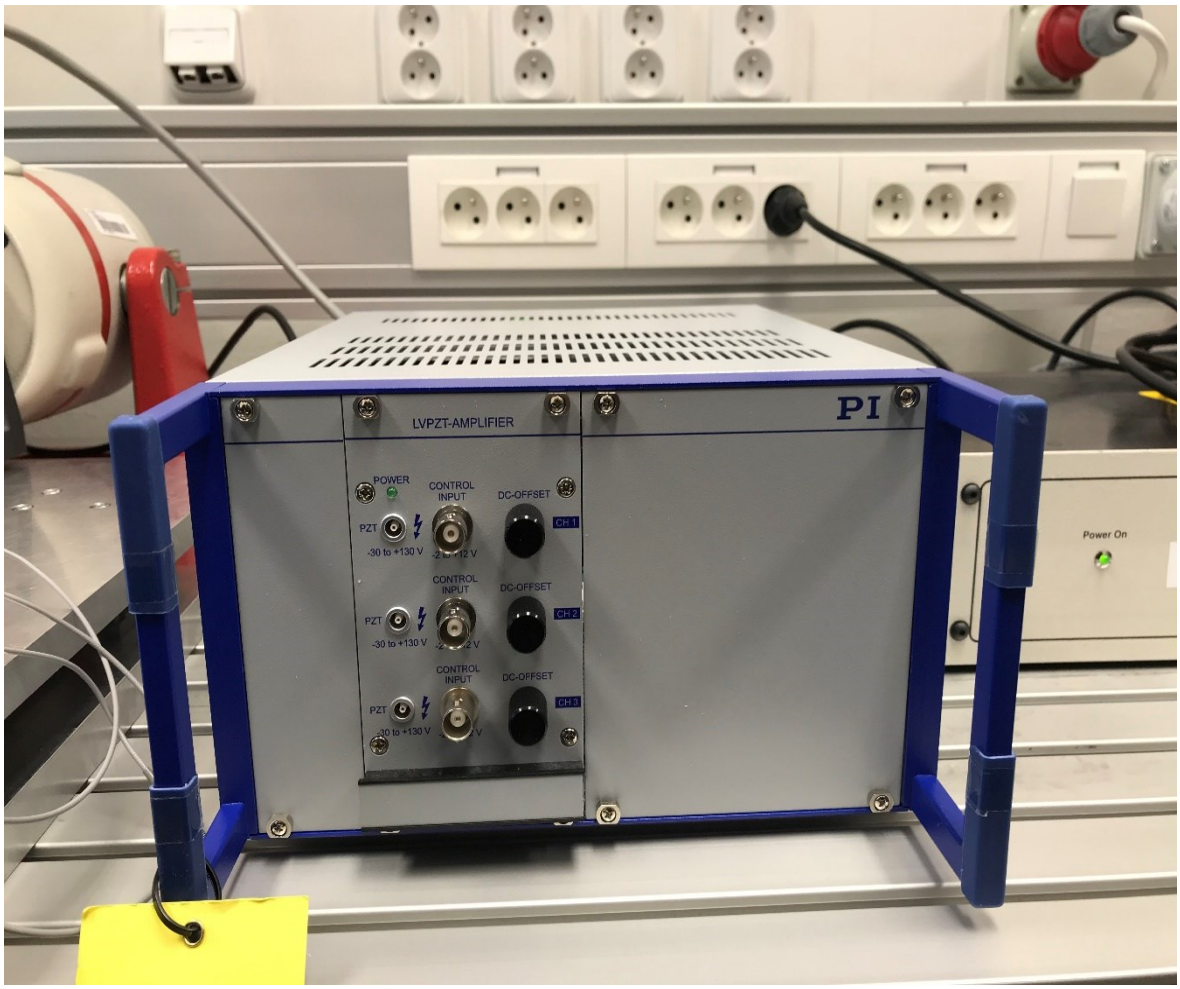

Figure 3.14 PI LVPZT Piezo power amplifier

Amplifiers / power amplifiers for piezo actuators have 0 V to 10 V operating voltage that is amplified to 0 V To 100 V in order to supply to piezo actuator. Since they have an offset knob to adjust the offset hence have -20 V to 120 V. Amplifiers with switchable power amplifiers are available for high dynamics. High linearity, also without position feedback, can be achieved with charge-control amplifiers. Amplifier modules are offered for one to three channels per module depending on the performance class.

3.11 ELECTRODYNAMIC SHAKER

The electrodynamic shakers are used for vibration testing. This device excites vibration to the device, equipment or the attachment. It is also used to test the mechanical wear and tear of the equipment as the vibration excited creates backward and forward motion of an object.

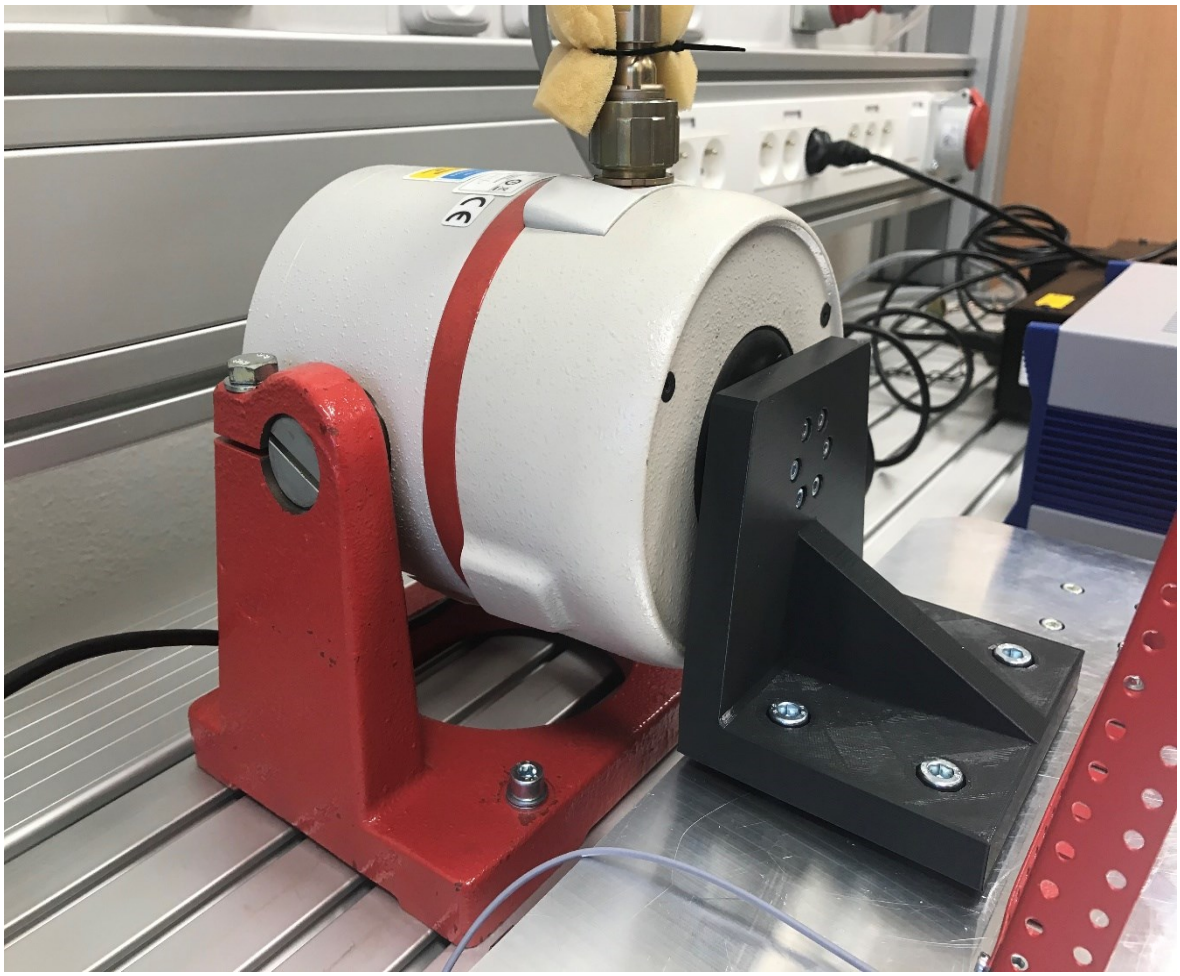

Figure 3.15 Electrodynamic shaker

The above image represents the electrodynamic shaker used which is connected to the connecter block that is interconnected with the upper plate which houses the structure. The vibration excited from the electrodynamic shaker creates to and motion of the upper plate and the vibrations are transmitted to the structure.

3.12 PIEZO ACCELEROMETER

The sensor used in for the experimentation is accelerometer. The Piezoelectric CCLD accelerometer type 4507-B-004 is used. The accelerometer is mainly designed for the model analysis measurements. The specification of the accelerometer used is given in the table below. (Bruel & Kjaer, 2020)

Table 3.1 Specification of the accelerometer used for the measurement

Frequency range	0.3 – 6000 Hz
Weight	4.6 g
Sensitivity	10 mV/ms^{-2}
Output	CCLD
Resonance frequency	18 kHz

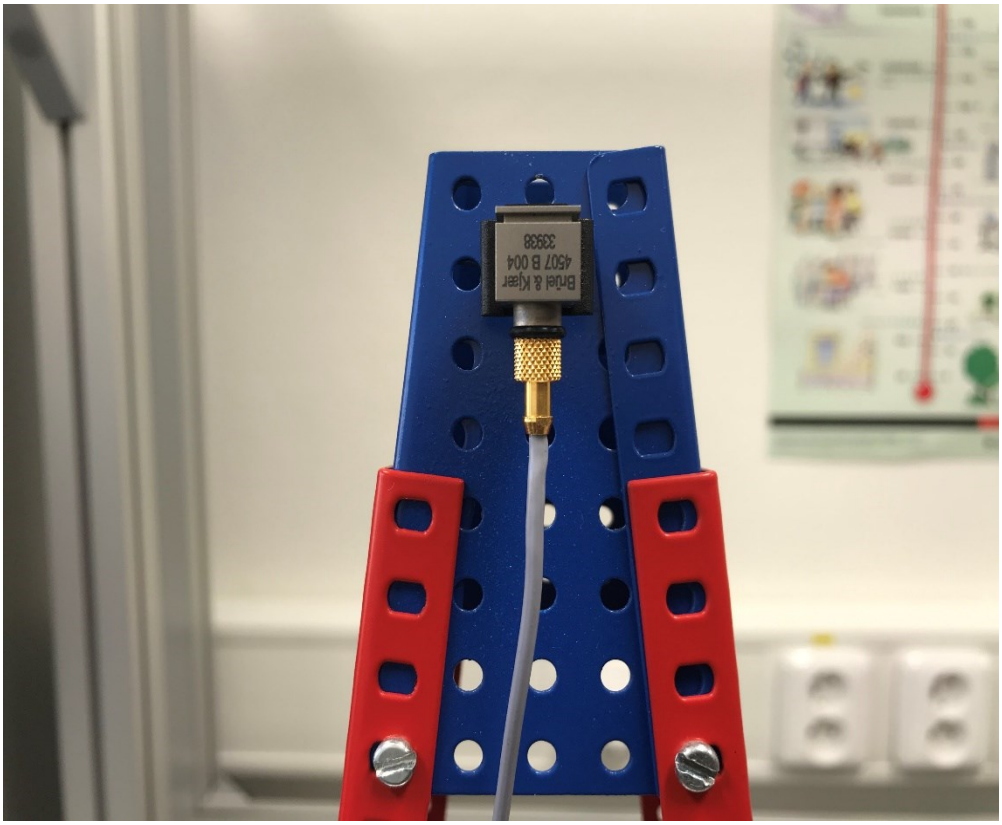

Figure 3.16 Piezo accelerometer attached to the structure

Piezo accelerometer is the type of accelerometer that works based on piezoelectric effect to measure the dynamic changes of mechanical variables like vibration, acceleration.

3.13 PIEZOELECTRIC ACTUATOR

The piezoelectric actuator uses piezoelectric materials as the active material. They have low displacements and are able to produce big forces.

The piezoelectric actuator used is P – 842.40. They have a travel range of 90 µm. The pushing force is up to 800 N and pulling force is up to 300 N.

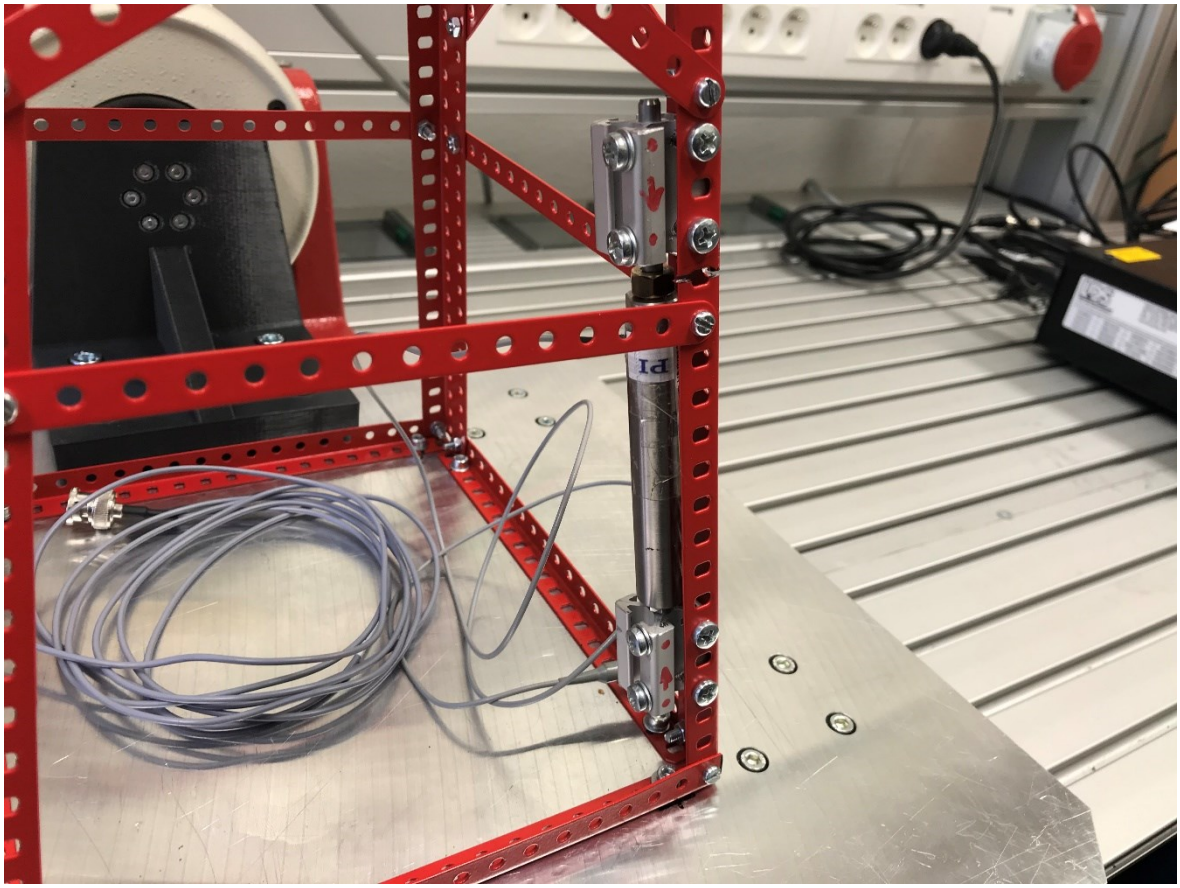

Figure 3.17 Piezoelectric actuator attached to the structure

The piezoelectric materials can transduce the mechanical energy to electrical energy and vice versa. When the piezo materials are subjected to an electrical field, produce mechanical strain which intern generates electricity in the material.

They can produce great forces and undergo mechanical strain or changes in dimension in form of electrical charge. The supply voltage to the piezo actuator is from 0 V to 100 V. The actuator is built into the structure.

3.14 CONTROL SYSTEM

The dSpace clp 1104 instrument was used to connect the system for the providing input to the power amplifier controlling the shaker and the piezo amplifier, the same instrument was also used to measure the vibrations and provide the control signal to the piezo amplifier which controls the piezo actuator to reduce the vibrations.

Figure 3.18 dSpace control system terminal CLP1104

It consists of sixteen ports in which there are eight input ports and eight output ports. It is used as a real-time interface where we can run the functions models on control board. The software dSpace software is used which provides visualization from the control algorithm designed using the Simulink in the MATLAB.

3.15 EXPERIMENTAL SETUP ASSEMBLY

The experimental setup of the designed parts is shown in this section of the document where the entire structure attached with piezo actuator and the accelerometer attached to the top mast is seen, the structure is intern connected to upper plate the linear guide block which is connected with the linear rails and the bottom plate attached to the table.

Figure 3.19 Experimental assembly of the designed parts

Further the dSpace instrument, power amplifier and piezo power amplifier is shown in the above Figure 3.19 which completes the laboratory model instruments used to measure and control the structure for the vibrations.

4 EXPERIMENTAL IDENTIFICATION OF THE SYSTEM

The experimental identification is done to identify the system and to know the characteristics of the system. The measurement of frequency response function of the shaker to accelerometer and the piezo to accelerometer was done to identify the system. Measurement of frequency response function using vibration excitation consists of several steps. The input and output signal are measured in the beginning. The signal is divided into number of realizations. These realizations are called blocks and each block has *N* number of samples. These blocks have overlay, which is traditionally 2/3. Each block is weighted by Hanning time window and weighted block is transformed using fast Fourier transform. Then we compute auto spectrum and Frequency response function (FRF).

4.1 FREQUENCY RESPONSE FUNCTION FROM SHAKER TO ACCELEROMETER

The frequency response function of the structure was executed and auto spectrum. Measurement was taken from the signal analyser Pulse Labshop software and the graphs were plotted using MATLAB software.

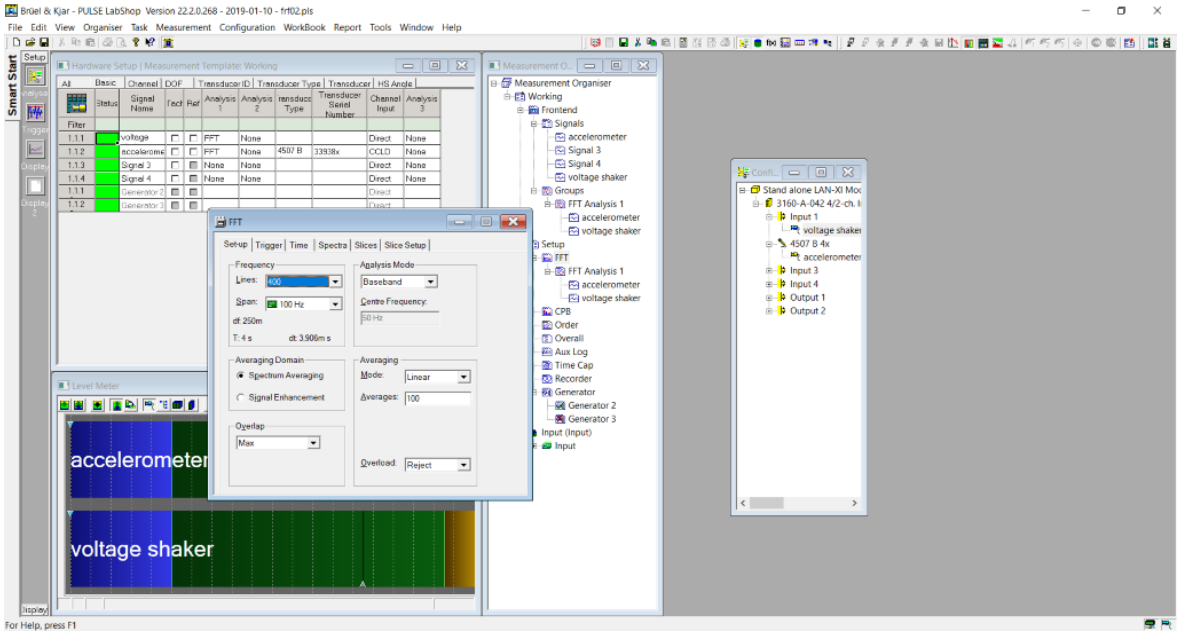

Figure 4.1 Bruel and Kjaer pulse Labshop software used to control output measure FRF

In this step the vibrations were excited from the electrodynamic shaker. The shaker was excited by connecting the power amplifier to the input port of the data acquisition module. The accelerometer used to measure the acceleration was connected to the input port of the signal generator. This data acquisition module was connected to the laptop using the RJ45 port to the system and the signal

generation was controlled using the Bruel and Kjaer Pulse Labshop software. The output from the signal generator is excited with white noise to the electrodynamic shaker to identify the system. The frequency response function is obtained in the frequency domain then we get it in Laplace domain during the approximation process.

The lines used in Fast Fourier Transform (FFT) were 1600 lines and the frequency used is 400 Hz. Hanning window is applied after that the overlap was set to maximum overlap to speed up the measurement process. The averaging mode was set to linear and spectrum averaging was used.

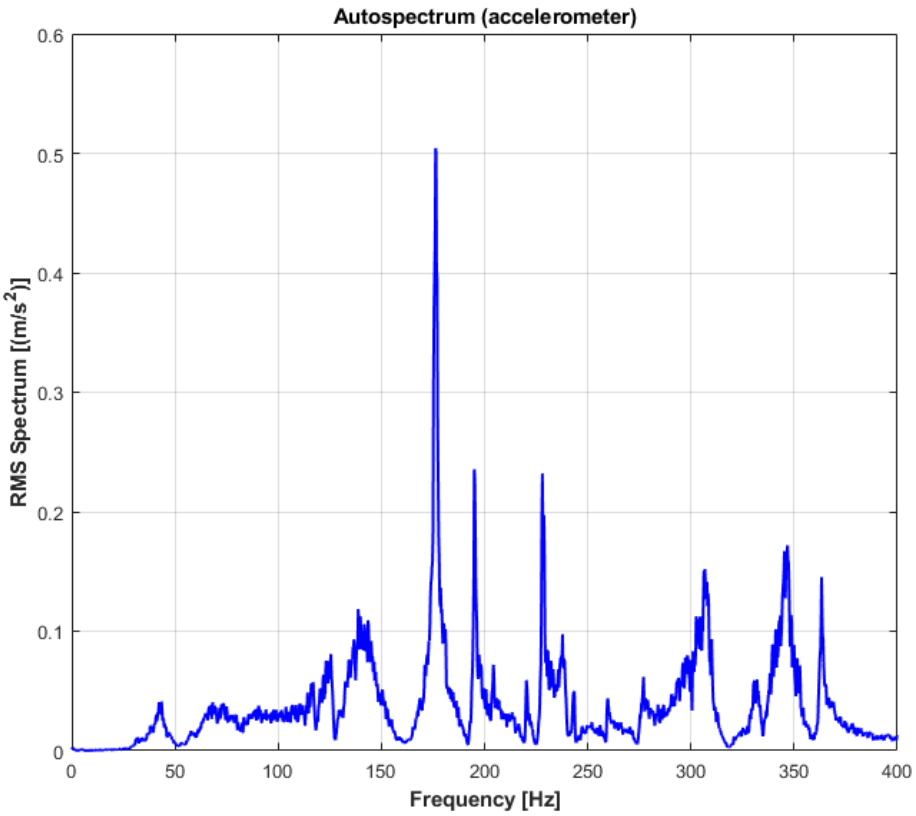

Figure 4.2 Auto spectrum (Accelerometer) input

The frequency range was set to 1600 Hz. The averages are also set to 400. In Figure 4.2 from 0 Hz to 26 Hz the RMS spectrum is zero, but we can see the small variations because high pass filter was used and we can observe the peaks at various frequencies like 139.8 Hz, 176.3 Hz, 195 Hz and so on but the resonant frequency peak is 176.3 Hz.

The Figure 4.2 shows what frequencies are in seen when the shaker is excited by white noise.

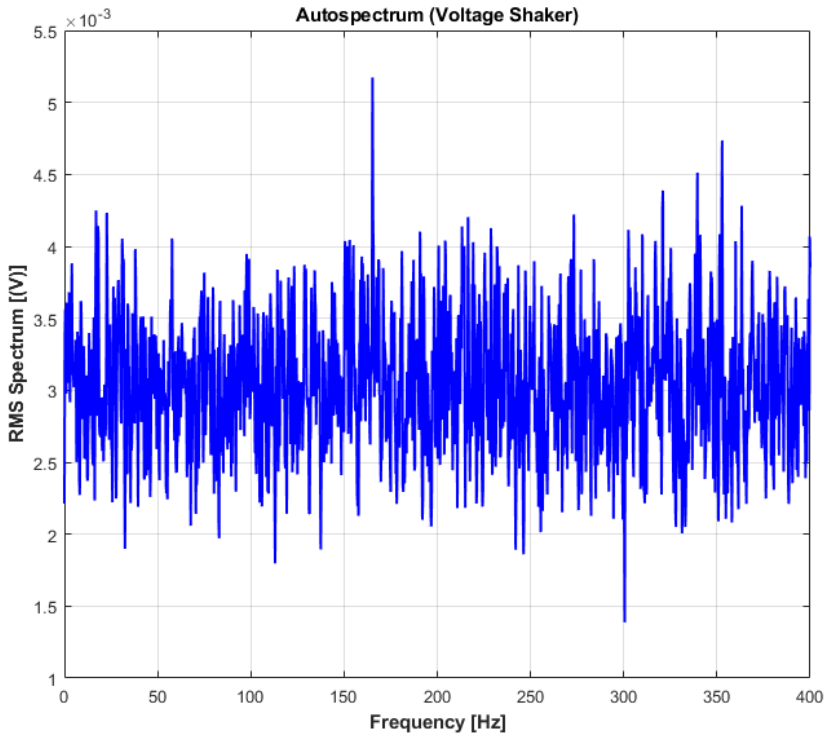

Figure 4.3 Auto spectrum (voltage shaker) input

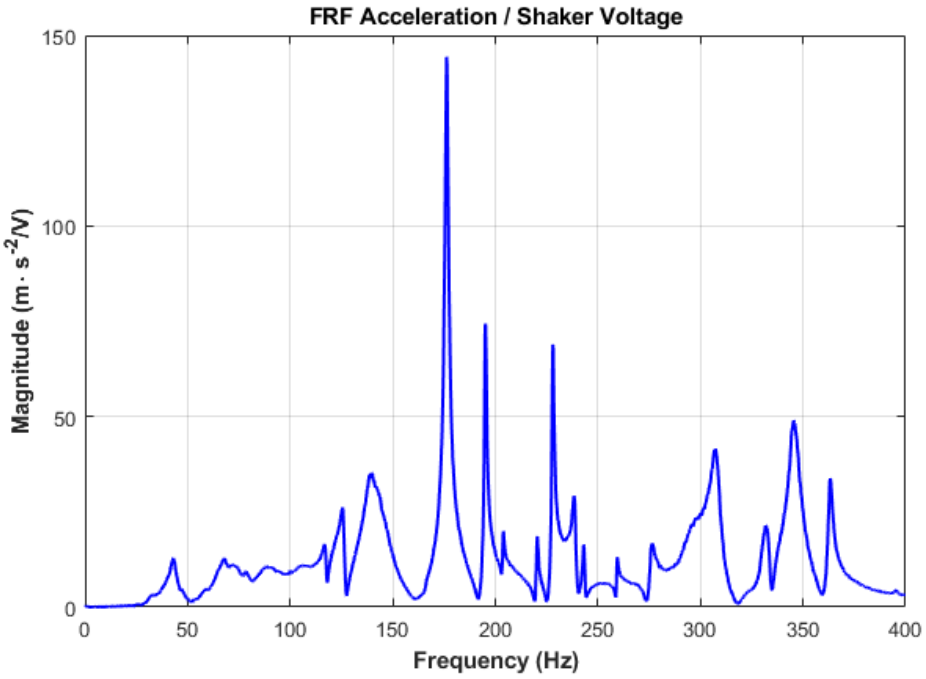

Figure 4.4 Frequency Response H1(accelerometer, voltage shaker) – Input

Since the constant power spectrum is used for excitation resonant frequencies are seen.

4.2 FREQUENCY RESPONSE FUNCTION PIEZO ACTUATOR AND ACCELEROMETER

The frequency response function from piezo to accelerometer was performed the same steps as mentioned in previous chapter 4.1. The difference is the measurement is made for piezo actuator and accelerometer rather than voltage shaker and accelerometer.

The graph of auto spectrum accelerometer, auto spectrum voltage piezo and frequency response function are plot and are given below in Figure 4.5, Figure 4.6 and Figure 4.7. The same inputs were set in Pulse Labshop.

The lines used in Fast Fourier Transform (FFT) were 1600 lines and the frequency used is 400 Hz. Hanning window is applied, the overlap was set to maximum overlap to speed up the measurement process. The averaging mode was set to linear and spectrum averaging was used.

We can observe the peaks at various frequencies like 138.5 Hz, 175.8 Hz, 195.3 Hz and so on but the resonant frequency peak is 175.8 Hz.

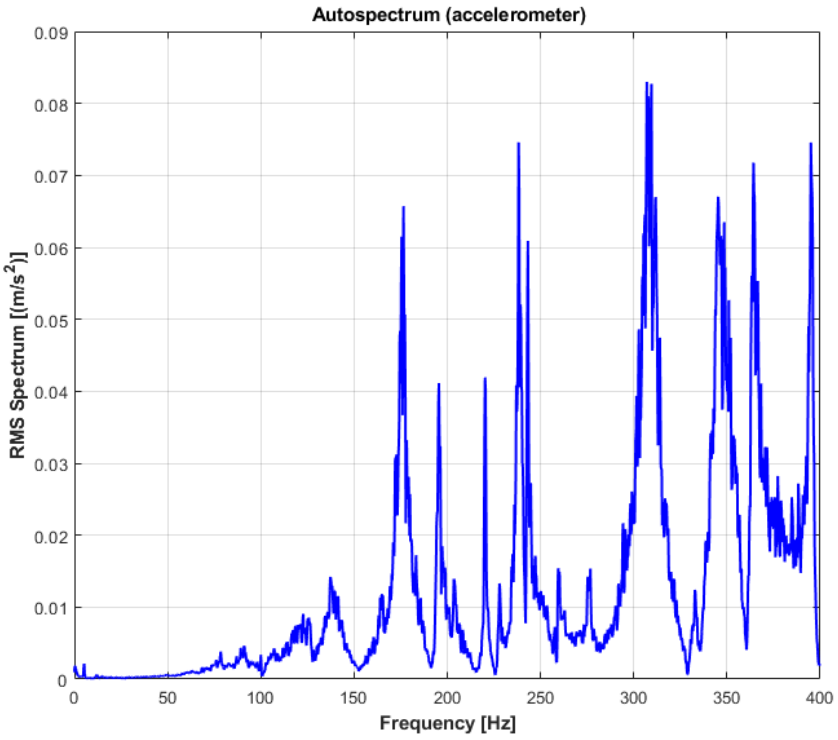

Figure 4.5 Auto spectrum(accelerometer) – Input

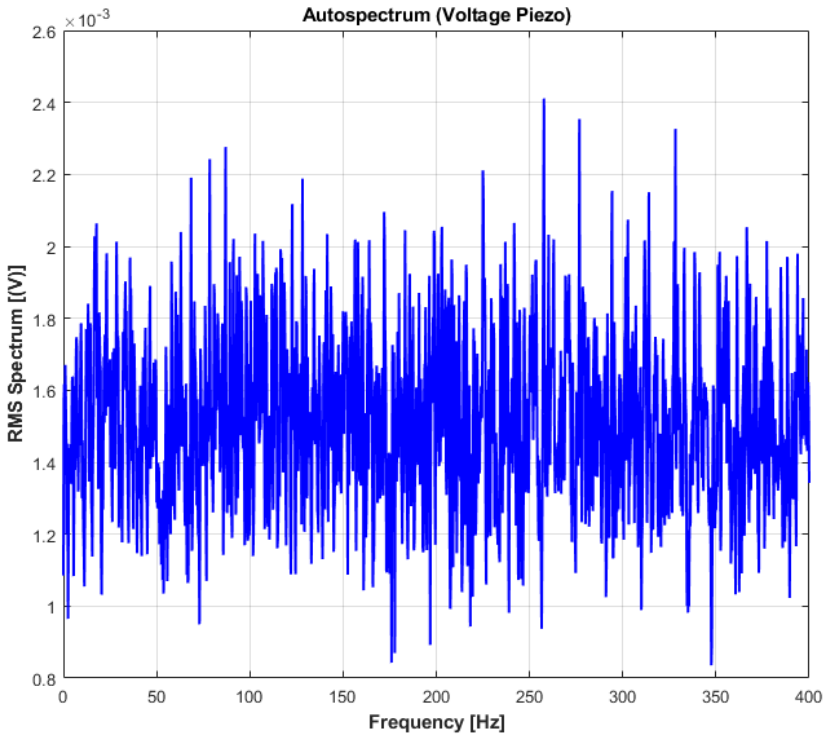

Figure 4.6 Auto spectrum (voltage piezo) – Input

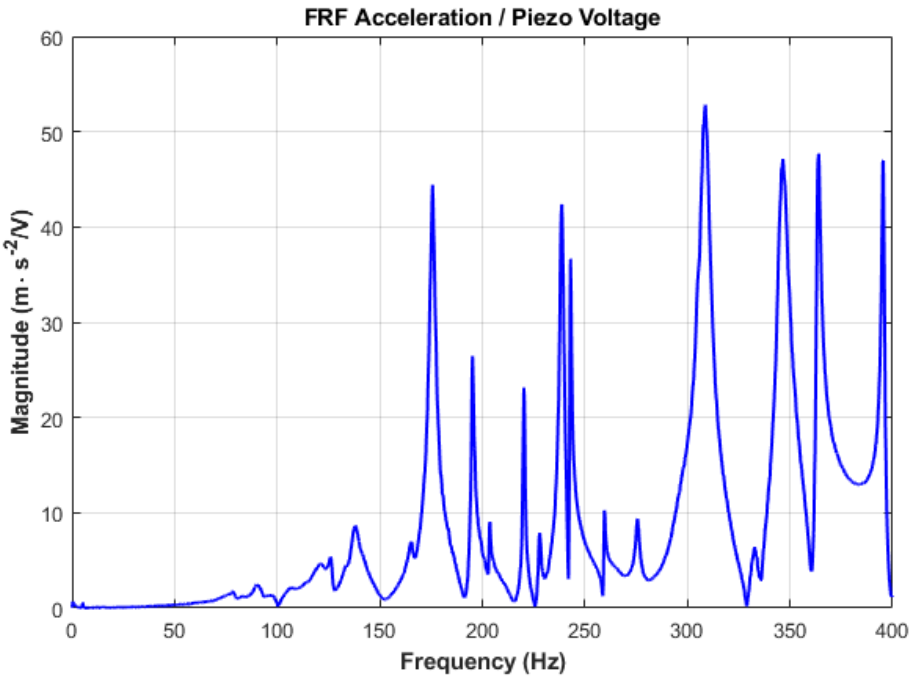

Figure 4.7 Frequency Response H1 (accelerometer, voltage piezo) – Input

5 APPROXIMATION

Approximation was done to obtain the transfer function for shaker to accelerometer from the frequency response function. The data obtained from the experiment in the form of text file from Pulse Labshop were inserted into MATLAB as input file. The text data was in matrix form hence we separated the matrix into individual complex numbers. This data was used to plot the frequency response function. The parameters were identified from the manual approximation these parameters were inserted to the calculation substitution in MATLAB to obtain the approximation transfer function.

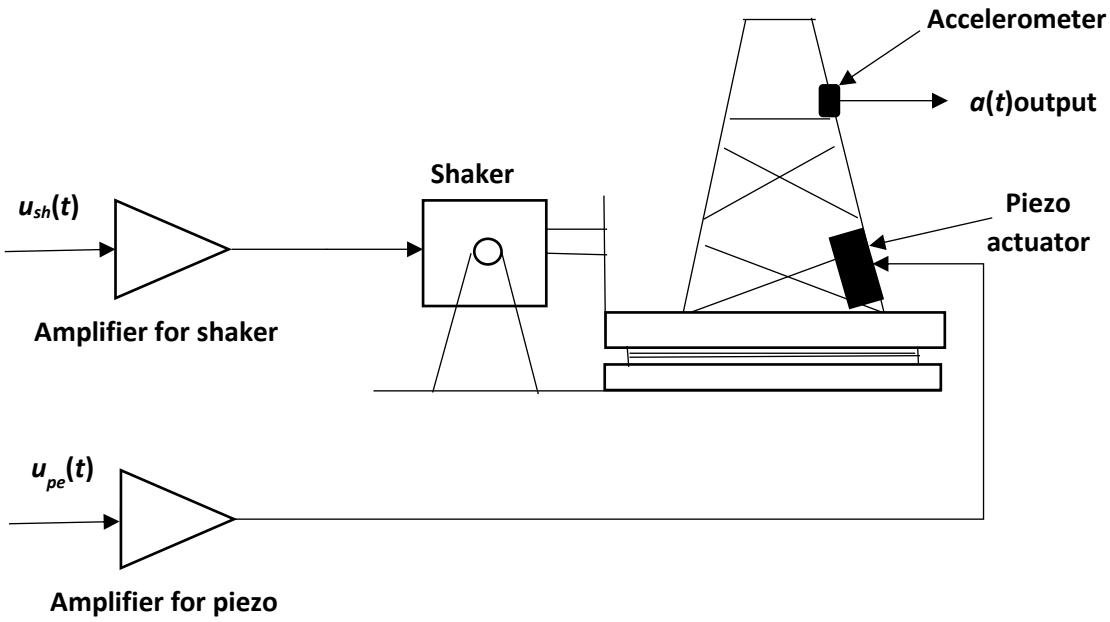

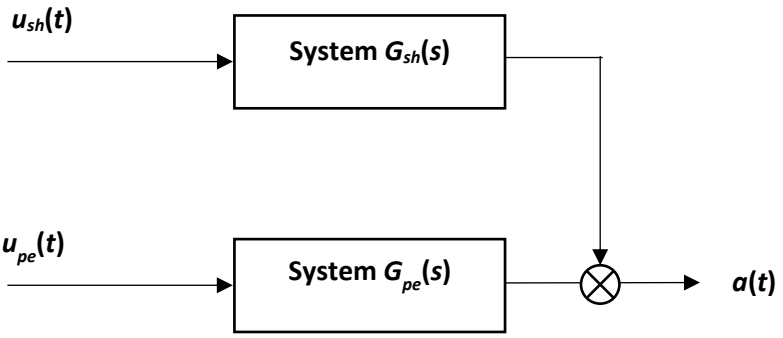

Figure 5.1 Sketch representation of input and output

The above sketch in Figure 5.1 shown in this chapter represent the input is given to amplifier in terms of voltage and the output is obtained in terms of acceleration from the accelerometer. Also, the input to piezo in terms of voltage is shown and the output is obtained in terms of acceleration.

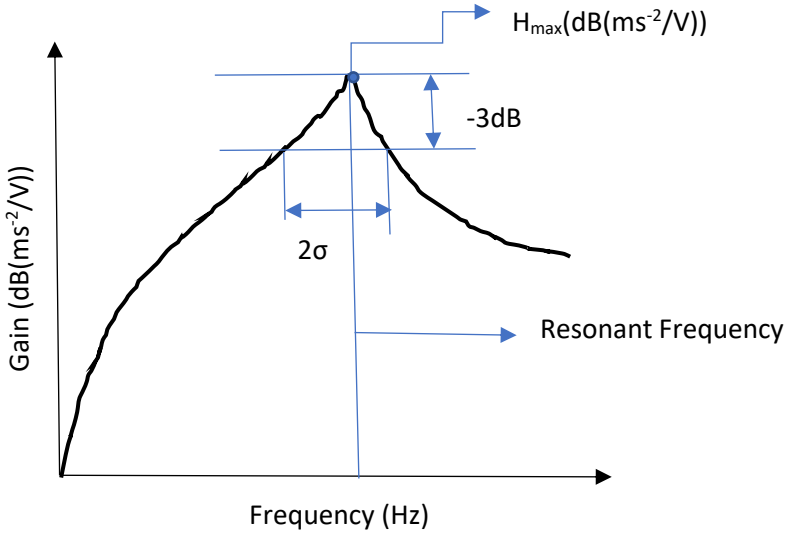

Figure 5.2 Frequency response plot drawn to show transfer function identification of shaker.

From the above Figure 5.2 we could obtain the form of transfer function for the frequency response function.

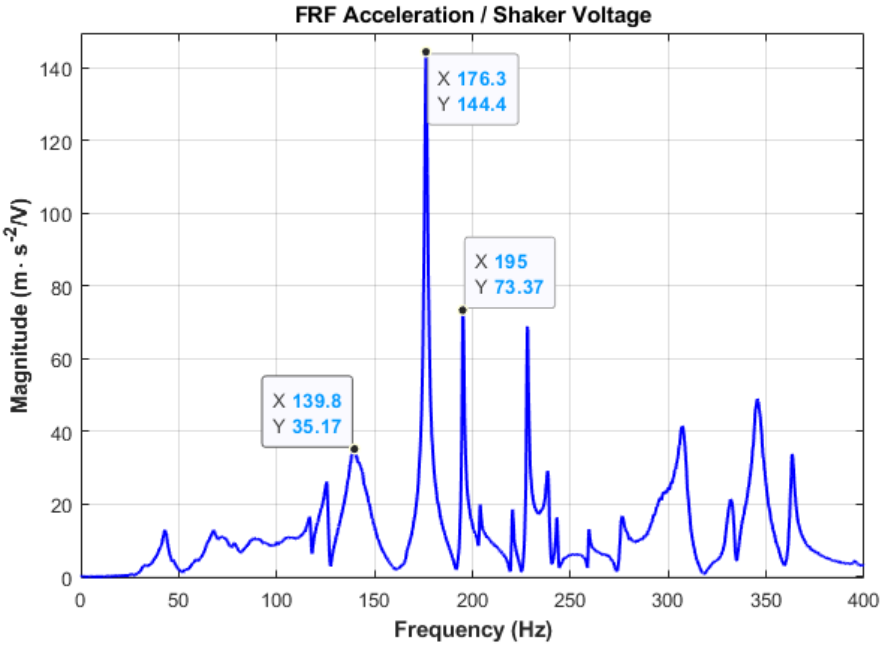

Figure 5.3 Three modes of FRF acceleration to shaker voltage selected for the identification and approximation

$$G_{sh}(s) = \frac{A\,s^2}{s^2 + 2\xi_0\omega_r s + \omega_r^2} \tag{5.1}$$

where the formulas of the individual components are given below

$$\xi_0 = \frac{\sigma}{f_r} \tag{5.2}$$

$$A = 2\xi_0 H_{max} \tag{5.3}$$

$$\omega_r = 2\pi f_r \tag{5.4}$$

For the 1st peak the bandwidth is σ = 4.50 Hz, resonant frequency f_r = 139.8 Hz, resonant maximum of the frequency response H_{max} = 35.17 m·s^{-2}/V. Hence damping ratio ξ_0 = 0.032, gain A = 2.2508 m·V^{-1} and frequency ω_r = 878.38 rad·s^{-1}.

From the above calculation and substitutions, we can write the transfer function from shaker to accelerometer as:

$$G_{sh1}(s) = \frac{-2.264\,s^2}{s^2 + 56.55s + 7.716 \cdot 10^5} \tag{5.5}$$

Then the graph was manually drawn on linear scale.

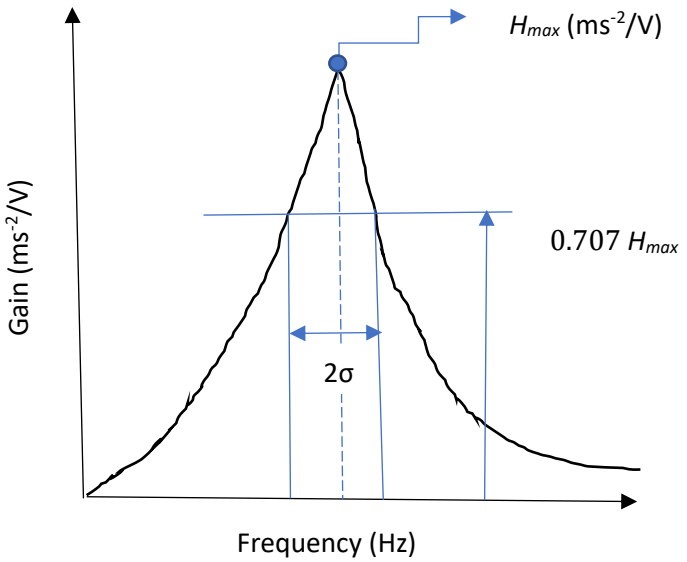

Figure 5.4 Manual plot drawn on linear scale for frequency response.

The manual drawing was drawn to represent the position of maximum frequency, resonant frequency and other symbols that are denoted in calculations used in equation 5.1-5.4. The Figure 5.5 and Figure 5.6 given in this chapter shows the approximated graph.

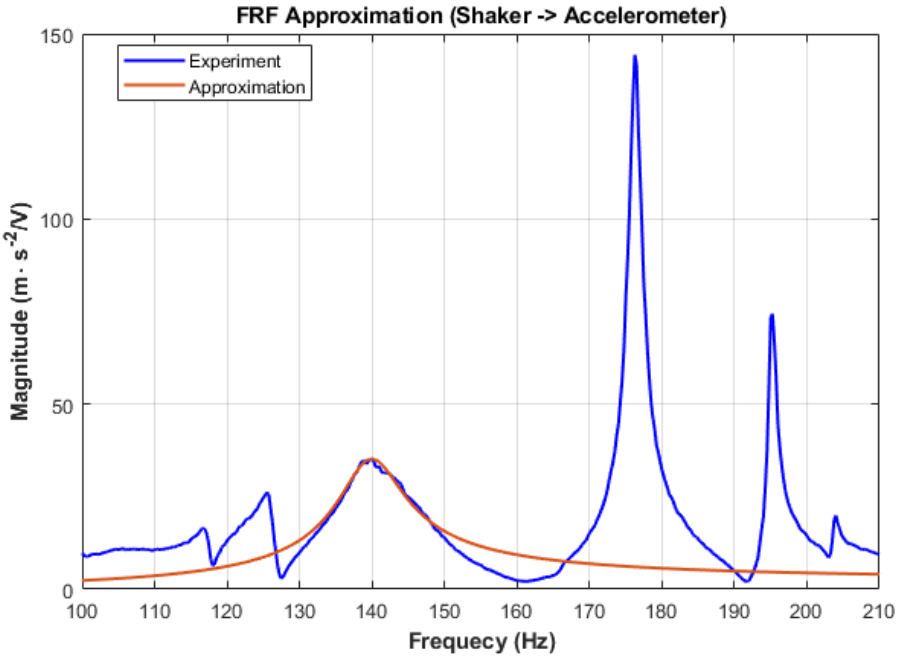

Figure 5.5 Approximated result of frequency response function for first frequency peak

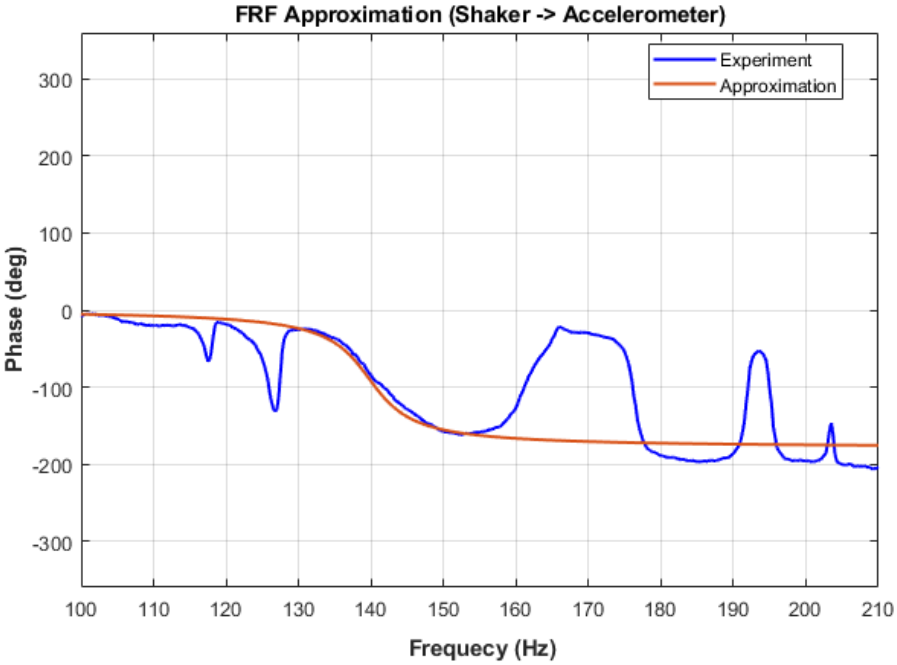

Figure 5.6 Frequency versus the phase plot for first frequency peak

For the 2nd peak the bandwidth is σ = 0.83 Hz, resonant frequency f_r = 176.3 Hz, resonant maximum of the frequency response H_{max} = 144.4 m·s^{-2}/V. Hence damping ratio $\xi_0 = 4.7078 \cdot 10^{-3}$, gain A = 1.3596 m·V^{-1} and frequency ω_r = 1107.72 rad·s^{-1}.

$$G_{sh2}(s) = \frac{-1.36\, s^2}{s^2 + 10.43s + 1.227 \cdot 10^6} \quad \textbf{(5.6)}$$

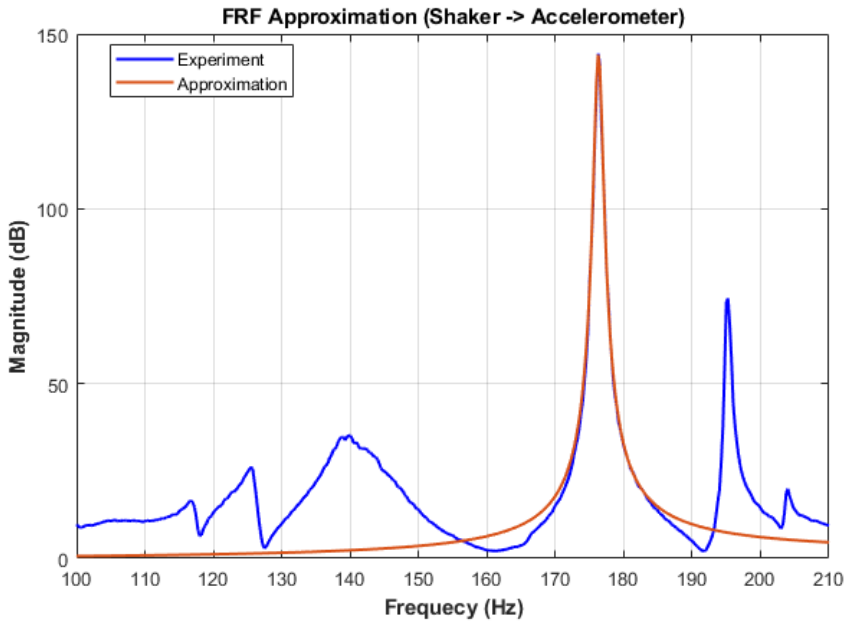

Figure 5.7 Approximated result of frequency response function for second frequency peak

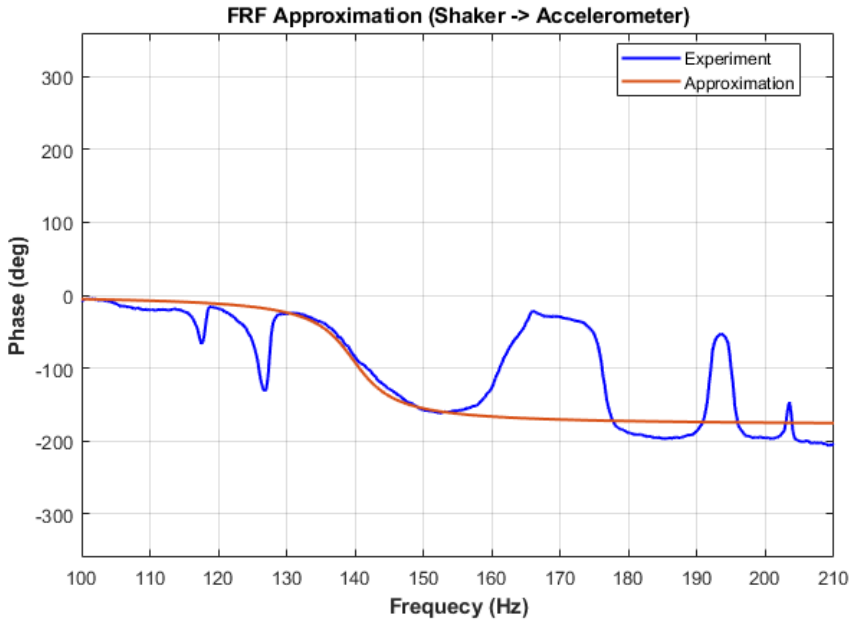

Figure 5.8 Frequency versus the phase plot for second frequency peak

For the 3rd peak the bandwidth is σ = 0.54 Hz, resonant frequency f_r = 195 Hz, resonant maximum of the frequency response H_{max} = 73.37 m·s^{-2}/V. Hence damping ratio ξ_0 = 2.7692·10^{-3}, gain A = 0.4063 m·V^{-1} and frequency ω_r = 1225.22 rad·s^{-1}.

$$G_{sh3}(s) = \frac{-0.4064\ s^2}{s^2 + 6.786\ s + \ 1.501 \cdot 10^6} \quad \textbf{(5.7)}$$

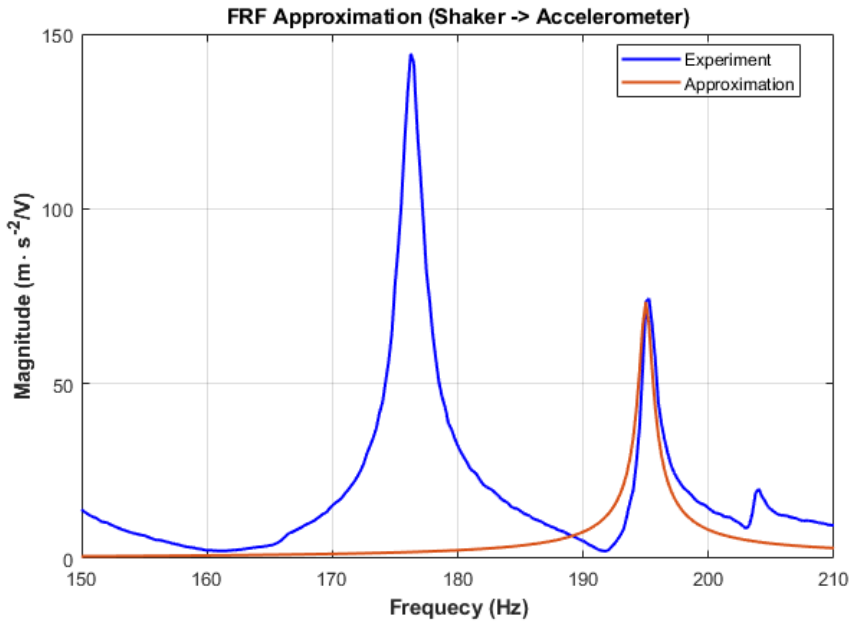

Figure 5.9 Approximated result of frequency response function for third frequency peak

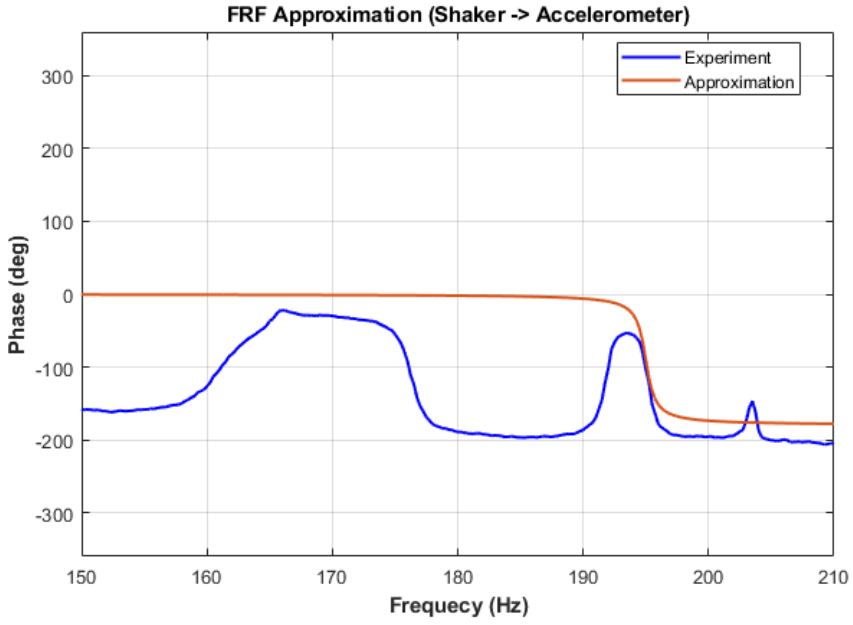

Figure 5.10 Frequency versus the phase plot for third frequency peak

The overall transfer function from shaker to accelerometer is given by the formula 5.8.

$$G_{sh}(s) = G_{sh1}(s) + G_{sh2}(s) + G_{sh3}(s) \quad \textbf{(5.8)}$$

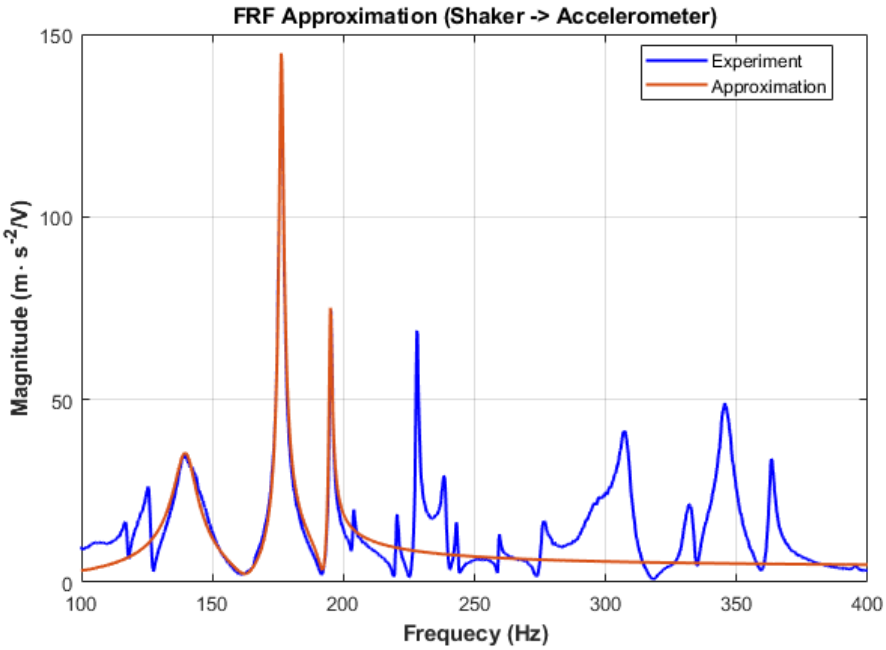

Figure 5.11 Approximated result of frequency response function

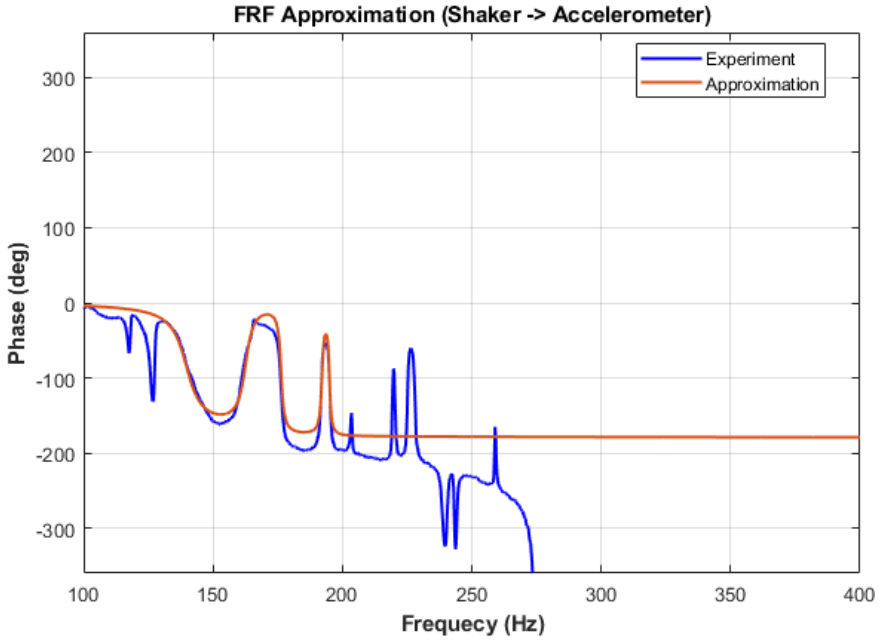

Figure 5.12 Frequency versus the phase plot

The identification and approximation processes were done the same way for the piezo to accelerometer in the similar way as shaker to accelerometer. The white noise signal was passed to the piezo actuator as the system input and the acceleration was the output from the accelerometer.

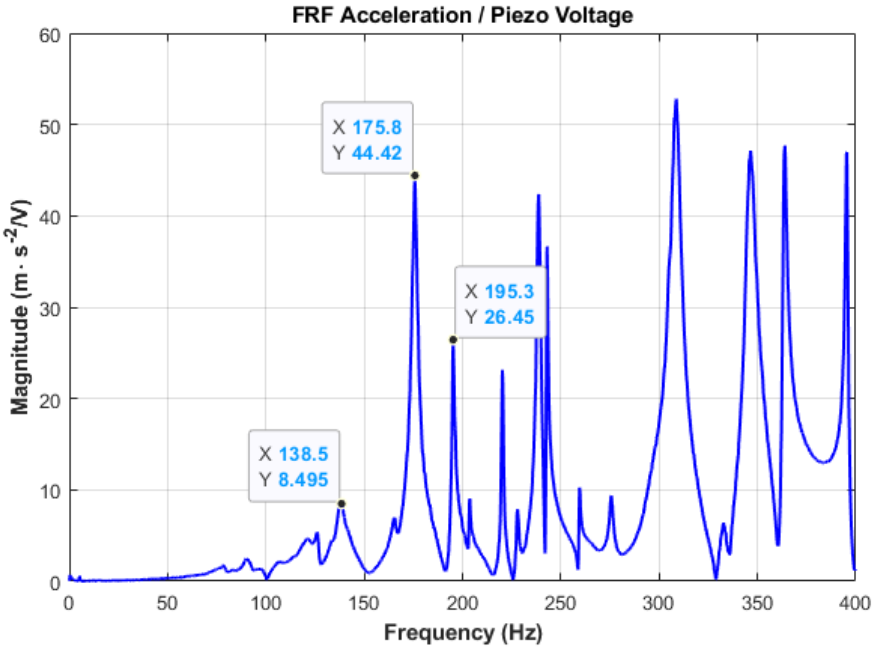

Figure 5.13 Three modes of FRF acceleration to piezo selected for the identification and approximation

$$G_{pe}(s) = \frac{A\,s^2}{s^2 + 2\xi_0\omega_r s + \omega_r^2} \tag{5.9}$$

The formulas for the individual components are the same which are mentioned from the equation number 5.2, 5.3 and 5.4 and the substitutions were done to the equation number 5.9 and the results were obtained.

For the 1st peak the bandwidth is σ = 2.42 Hz, resonant frequency f_r = 138.5 Hz, resonant maximum of the frequency response H_{max} = 8.495 m·s^{-2}/V. Hence damping ratio ξ_0 = 0.0174, gain A = 0.2968 m·V^{-1} and frequency ω_r = 53.3756 rad·s^{-1}.

$$G_{pe1}(s) = \frac{-0.2969\,s^2}{s^2 + 30.41\,s + 7.573 \cdot 10^5} \tag{5.10}$$

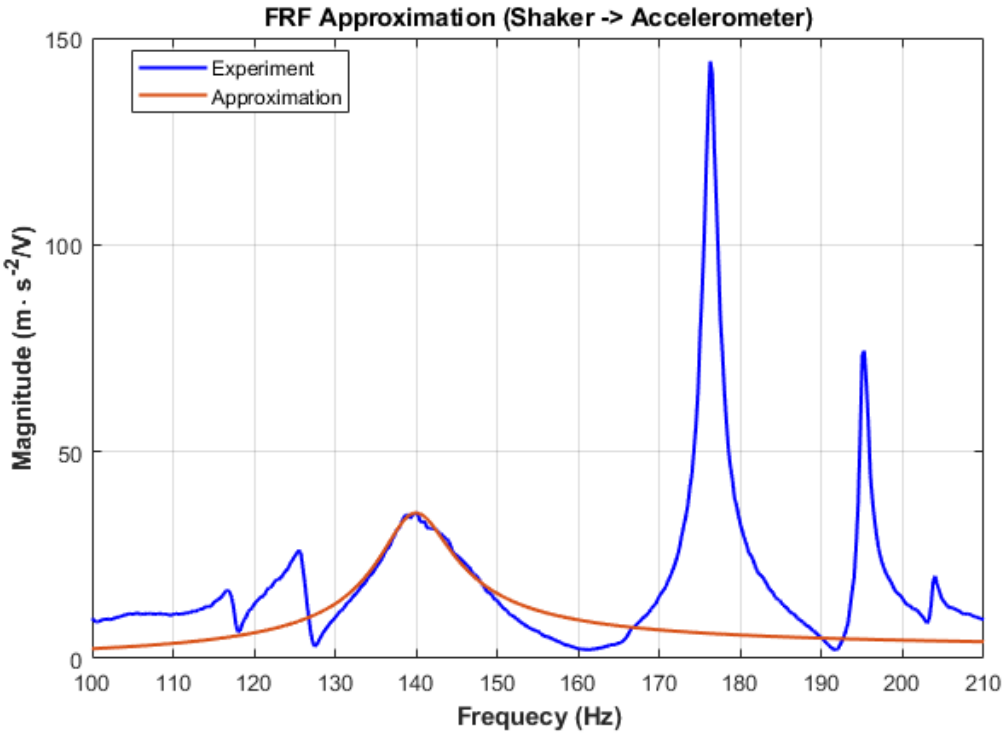

Figure 5.14 Approximated result of frequency response function for first frequency peak

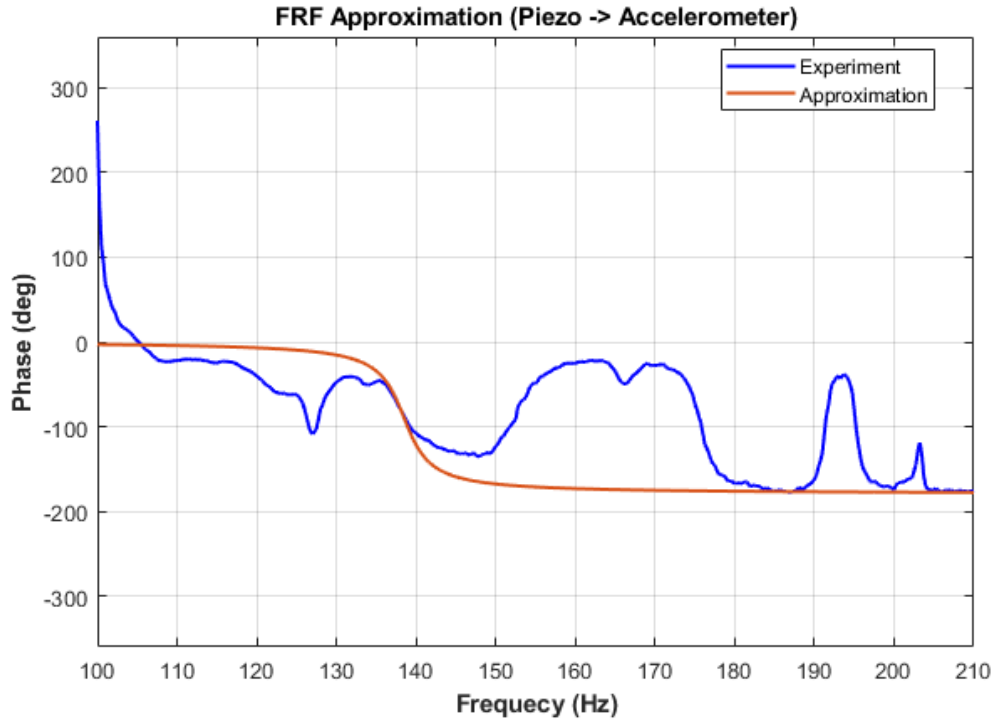

Figure 5.15 Frequency versus the phase plot for first frequency peak

For the 2nd peak the bandwidth is σ = 1.32 Hz, resonant frequency f_r = 175.8 Hz, resonant maximum of the frequency response H_{max} = 44.42 m·s^{-2}/V. Hence damping ratio ξ_0 = 7.5085·10^{-3}, gain A = 0.6670 m·V^{-1} and frequency ω_r = 1104.58 rad·s^{-1}.

$$G_{pe2}(s) = \frac{-0.6671s^2}{s^2 + 16.59\,s + 1.22 \cdot 10^6} \quad \textbf{(5.11)}$$

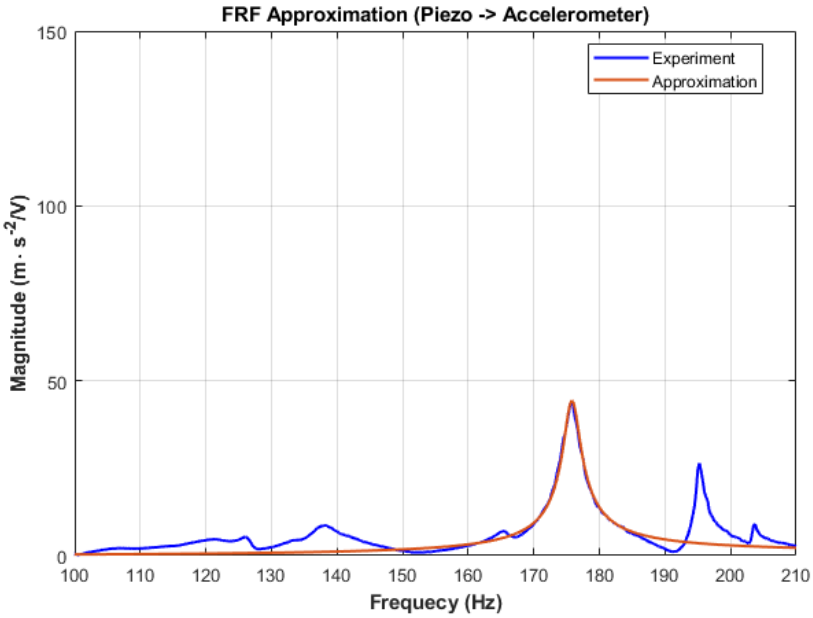

Figure 5.16 Approximated result of frequency response function for second frequency peak

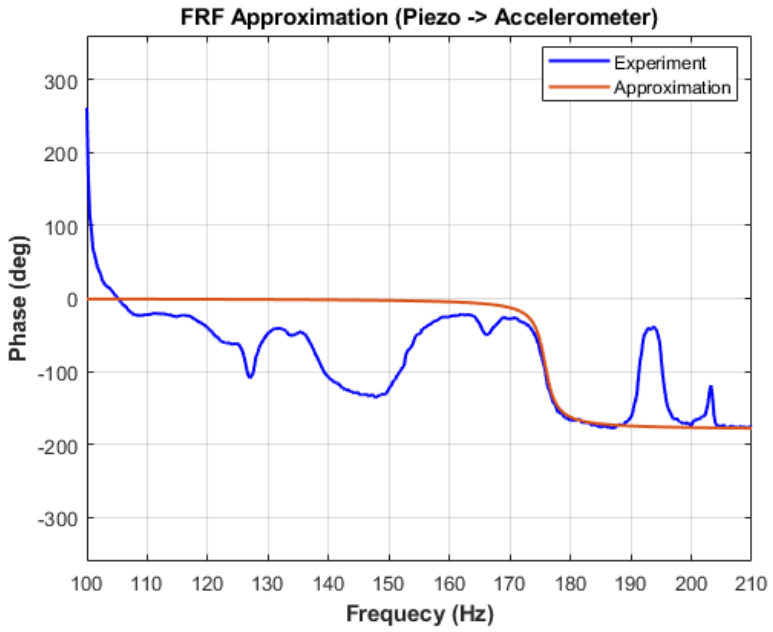

Figure 5.17 Frequency versus the phase plot for second frequency peak

For the 3rd peak the bandwidth is $\sigma = 0.59$ Hz, resonant frequency $f_r = 195.25$ Hz, resonant maximum of the frequency response $H_{max} = 26.45$ m·s^{-2}/V. Hence damping ratio $\xi_0 = 3.0217 \cdot 10^{-3}$, gain $A = 0.1598$ m·V^{-1} and frequency $\omega_r = 1226.79$ rad·s^{-1}.

$$G_{pe3}(s) = \frac{-0.1599\ s^2}{s^2 + 7.414\ s + 1.505 \cdot 10^6} \quad \textbf{(5.12)}$$

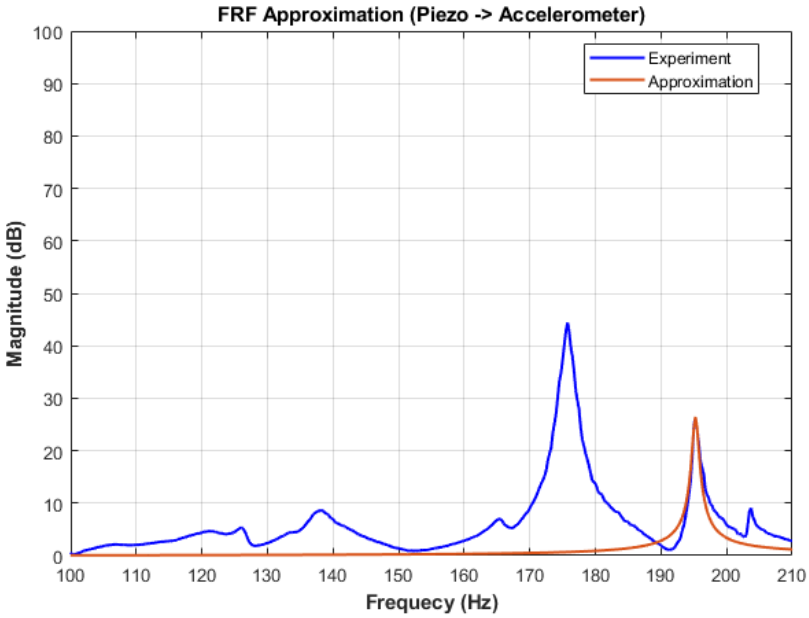

Figure 5.18 Approximated result of frequency response function for third frequency peak

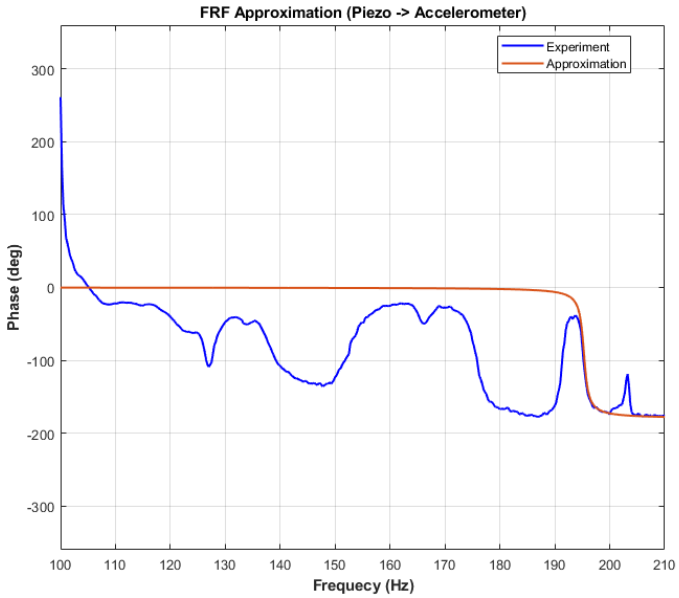

Figure 5.19 Frequency versus the phase plot for third frequency peak

The overall transfer function from shaker to accelerometer is given by formula 5.13.

$$G_{pe}(s) = G_{pe1}(s) + G_{pe2}(s) + G_{pe3}(s) \quad \textbf{(5.13)}$$

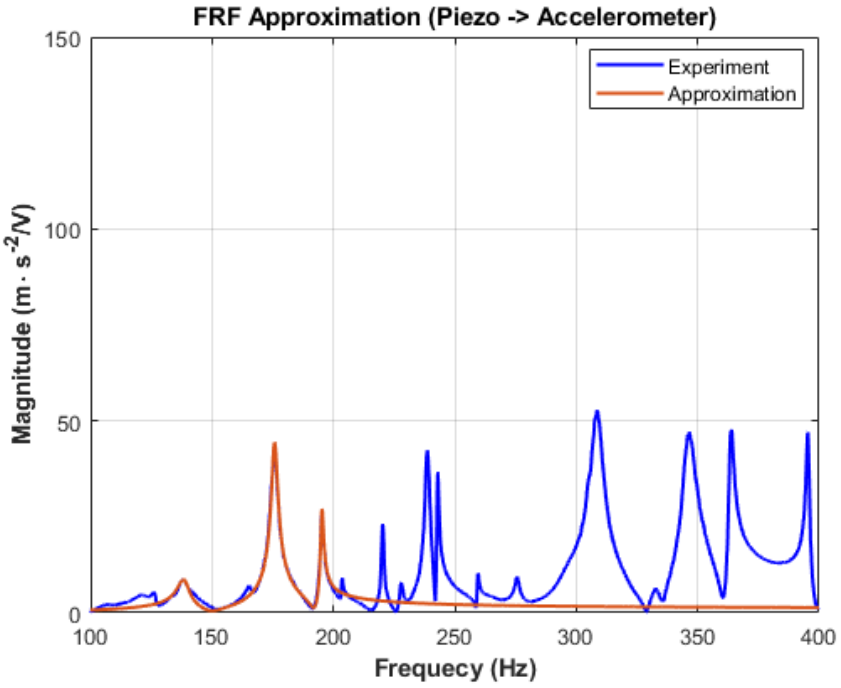

Figure 5.20 Approximated result of frequency response function

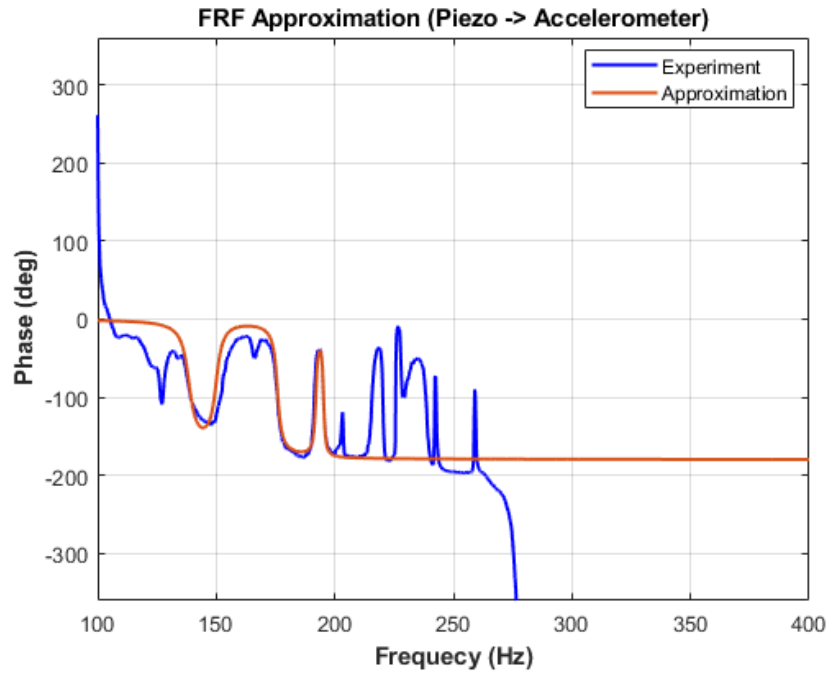

Figure 5.21 Frequency versus the phase plot

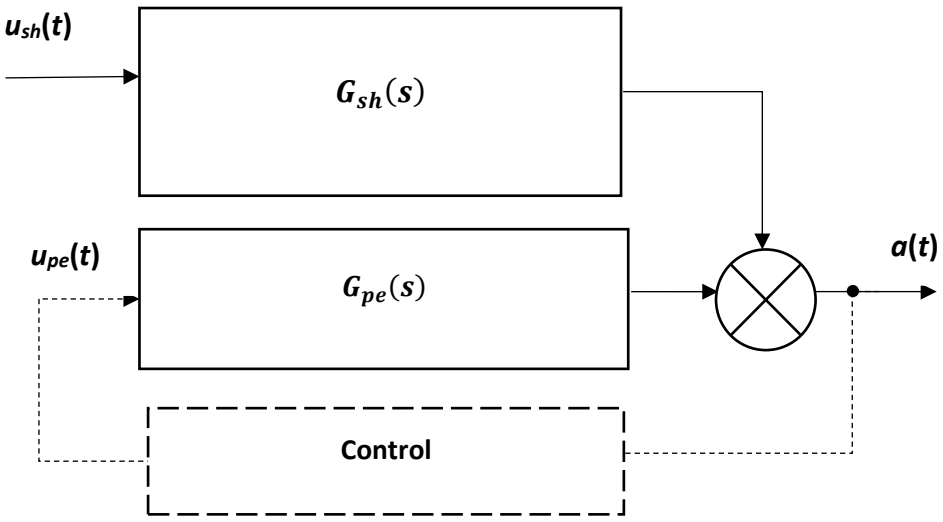

Figure 5.22 Block diagram of the identification

Figure 5.22 gives the block diagram of identification which shows the input and output and how the block is connected. The transfer function of shaker obtained by identification and approximation and the identification is done as stated above where white noise is sent as input signal and from the frequency response obtain the transfer function of shaker. The shaker acts as disturbance to the system.

The transfer function of the piezo is obtained by identification and approximation and the identification is done as stated above where white noise is sent as input signal and from the frequency response obtain the transfer function of piezo.

The feedback algorithm is explained in the next chapter and the velocity feedback control was selected to control the vibrations.

6 DESIGN OF CONTROL ALGORITHM AND IMPLEMENTATION TO THE LABORATORY MODEL

The Control algorithm designed using MATLAB Simulink tool which works on the direct velocity feedback control. The structure is excited by input signal, which is harmonic signal, which frequency is set to the resonant peak frequencies of the three modes selected in the simulation. The AVC is activated automatically after two seconds using the switch used. The acceleration is converted to the velocity by the integrator block used and this value is then amplified using gain block 150 times and sent as input voltage into the block of piezo actuator which is used to control and reduce the vibrations.

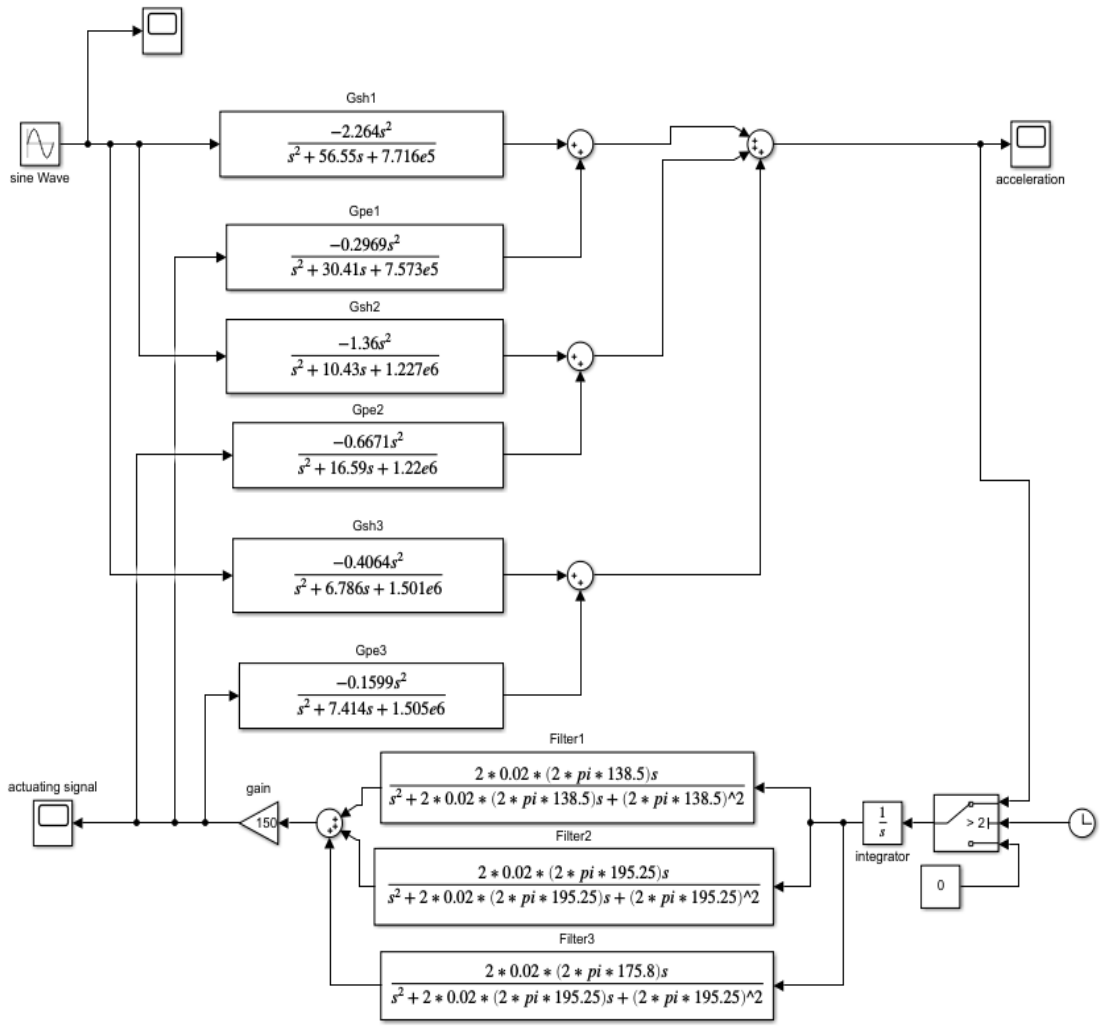

Figure 6.1 Control algorithm Simulink scheme representing the laboratory model

The Figure 6.1 represents the Simulink scheme which shows the input signal as harmonic signal, the transfer function blocks where the transfer functions are set as that obtained from the approximation. The output is acceleration, the switch is connected in the feedback loop with the

clock set to two seconds to activate the AVC after two seconds. Then the integrator is shown whose function here is to transfer acceleration to velocity after which the gain block is shown that represents the amplification of 150 times and then is sent as input voltage to the piezo actuator transfer function blocks.

Then the control algorithm was used in the MATLAB dSpace for connecting the working laboratory model to test for the control algorithm.The shaker was connected to ADC5 block which is the input to read the output signal from the shaker and the shaker was connected to DAC2 to control the input to shaker which is sine wave. Then the block is multiplied by the gain of 10 as the input is multiplied by 1/10 for the output to be 1 and then the block is multiplied by acceleration sensitivity as the accelerometer in the data manual has this value for the calibration, which is later multiplied by the m32 gain block which represents the physical gain block we use. The integrator is used to convert from acceleration to velocity and the is passed to the band pass filter which filters the unwanted frequencies and then the block is connected to DAC3 which is the input to the piezo.

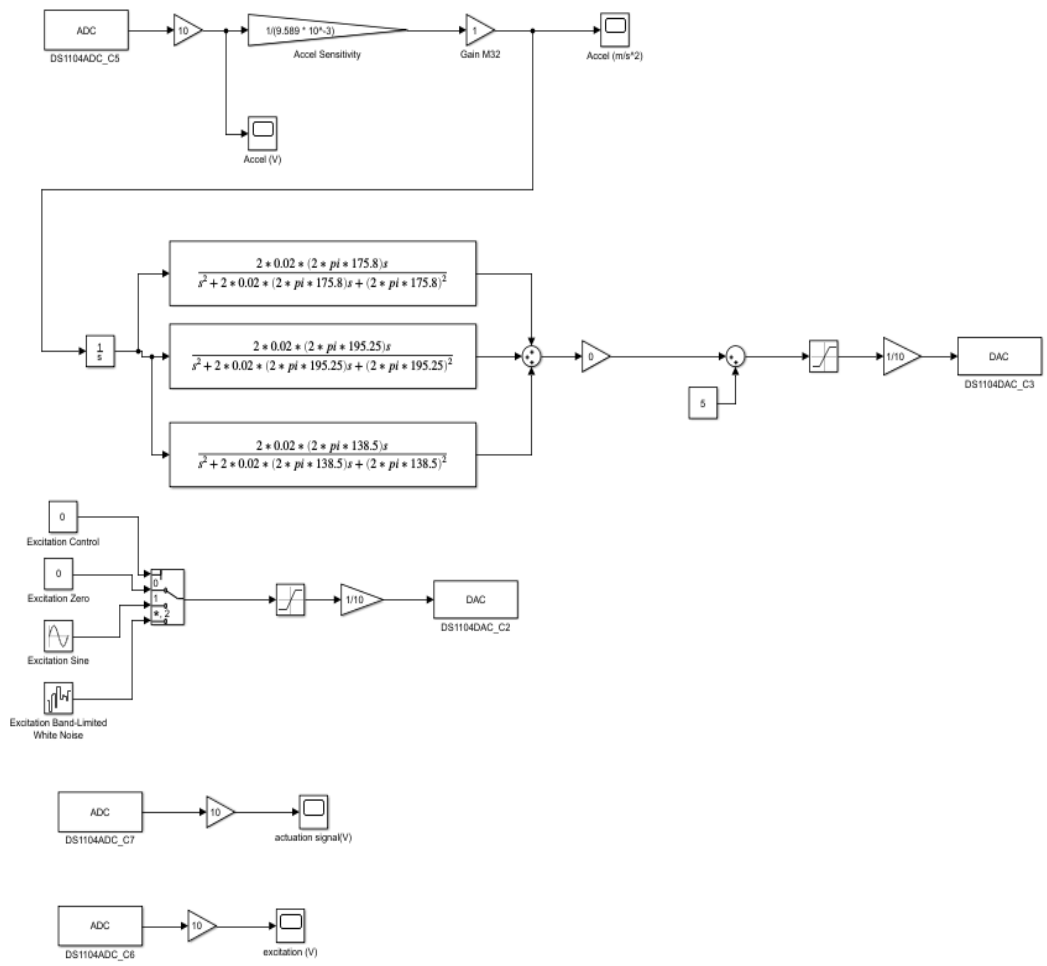

Figure 6.2 MATLAB dSpace implementation of control algorithm

The frequencies of the three filters are obtained from the identification of resonant frequencies of the piezo actuator. The excitation sine wave is fed as the input the shaker where the frequencies set are that of the resonant frequency of the shaker which was obtained from the identification of the shaker frequency response function.

Then we used dSpace control desk where we start taking the measurements and the visualization is seen through this and we obtain the readings of the measurements using this tool later which the reading is imported to the MATLAB, In MATLAB we analyse and process the readings obtained from the dSpace control desk.

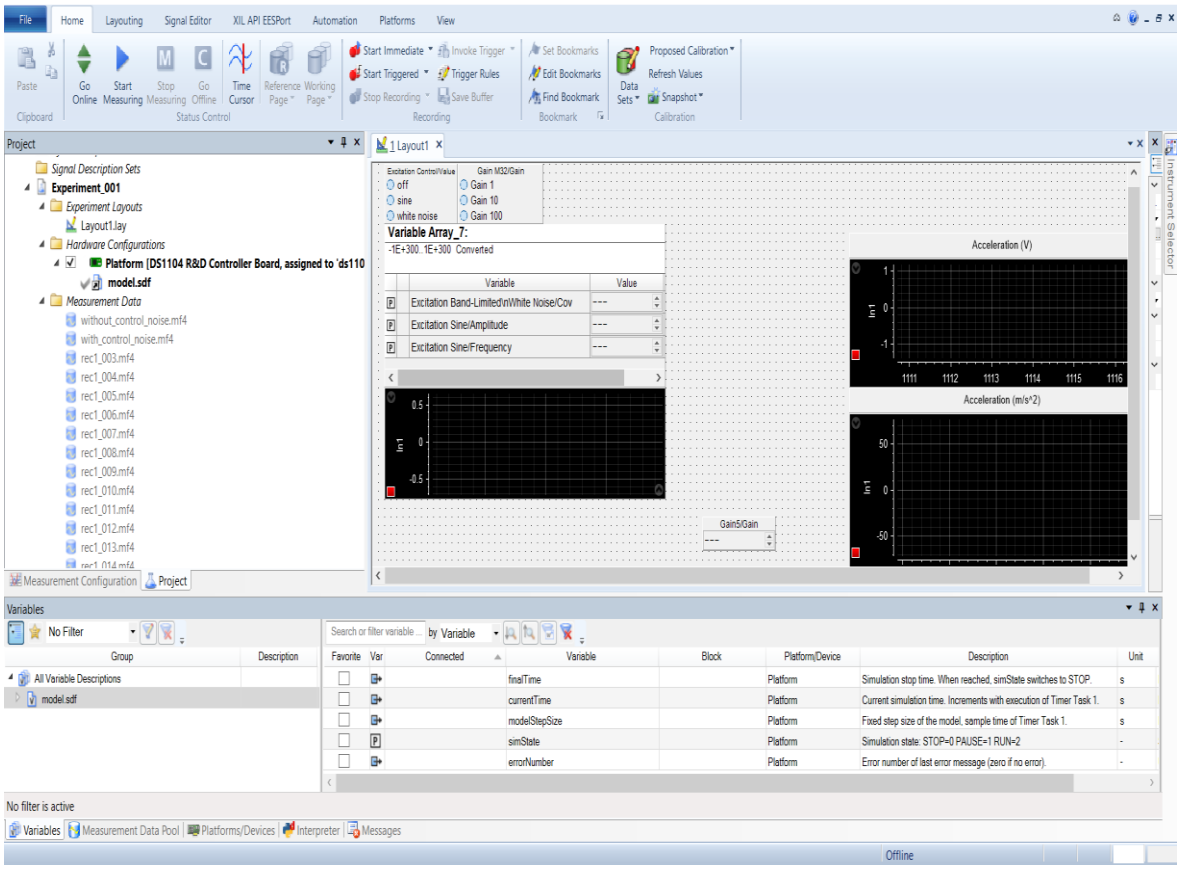

Figure 6.3 Screenshot of the visualization tool used dSpace control desk

The first block shows the type of excitation and has a switch to turn off the input. The second block shows the setting of the gain block and the below which we can see the variable and the value where we feed the input frequency in terms of radians per second which is obtained by multiplying the frequency in Hz by 2π. Then the graph of the input signal is displayed below. On the right side the first graph shows the output from the accelerometer in terms of voltage and the below one shows the output of the accelerometer in terms of meters per second square.

7 RESULTS

The summary of the achieved efficiency of the control algorithm designed are explained and the experiment is designed same as the simulation showed in the previous chapter. Algorithm is using band pass filter to select the desired mode of vibration to avoid the excitation of the unstable modes.

The results of the first mode are shown below.

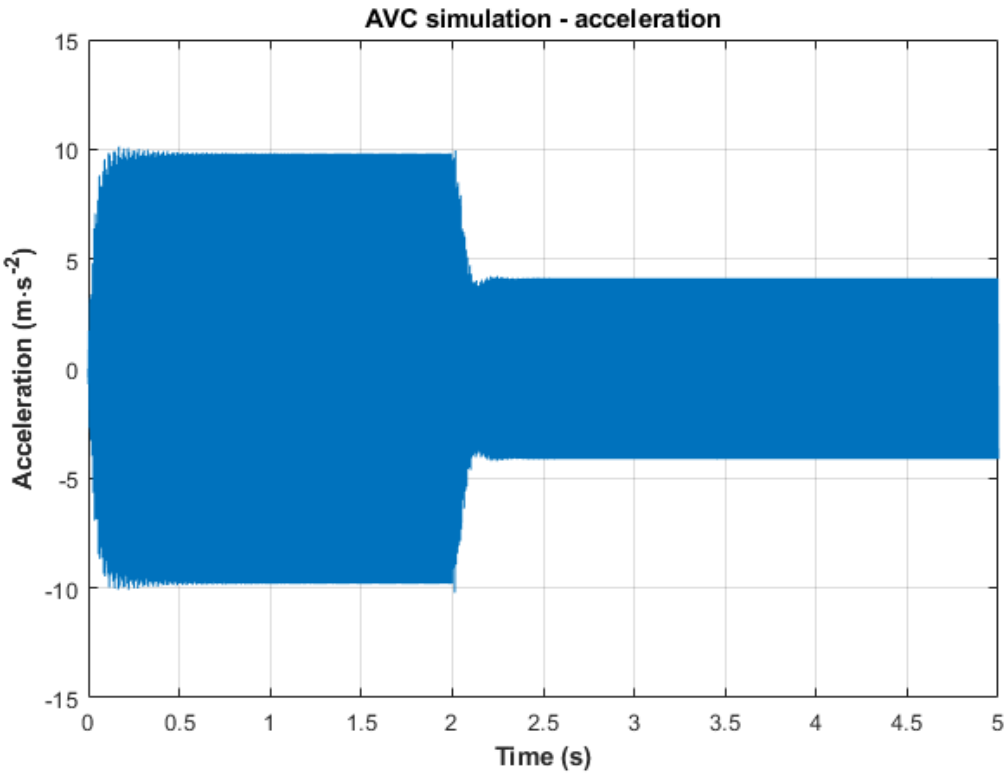

Figure 7.1 Time capture of acceleration for the first mode

The first mode had an excitation frequency of 139.8 Hz and from the graph we can observe the acceleration is 10 m/s^2 before the AVS is turned on and the acceleration reduces to 4.5 m/s^2. The AVC is turned on after 2 seconds automatically as we use the clock with 2sec timer to turn on the AVC switch.

The Figure 7.2 represents the actuating signal to the piezo and we can see increase in the actuating signal voltage when the AVC is turned on. The actuation signal to the piezo increases as the piezo actuator vibration acts in the opposite way to that of the shaker and provides the control force required to reduce the vibrations.

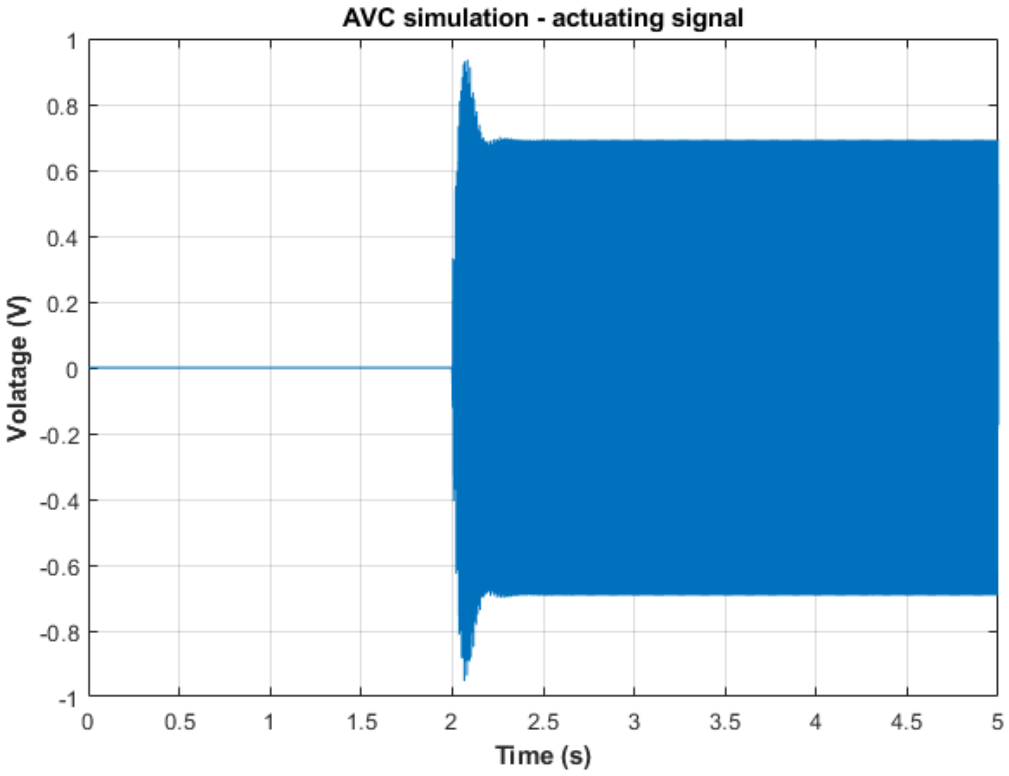

Figure 7.2 Time capture of actuating signal for first mode

The Figure 7.3 in which the blue portion in graph represents when AVC is turned off and the excitation is off and the red portion indication with the excitation to shaker turned on and AVC off and the Green portion represents the AVC turned on and the excitation to the shaker turned on.

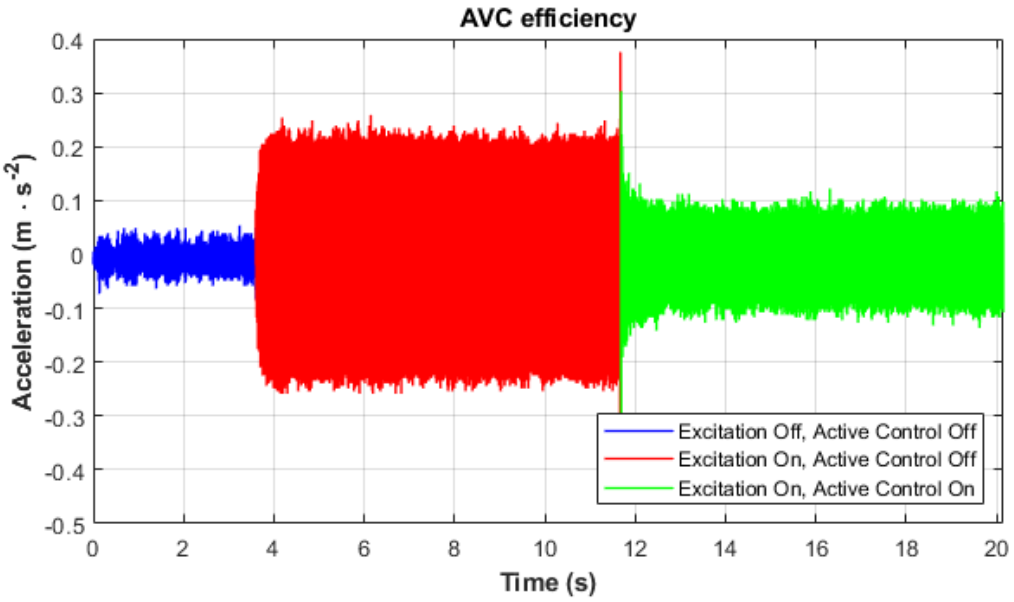

Figure 7.3 Time capture of top mast acceleration for first mode during switching on and off the AVC

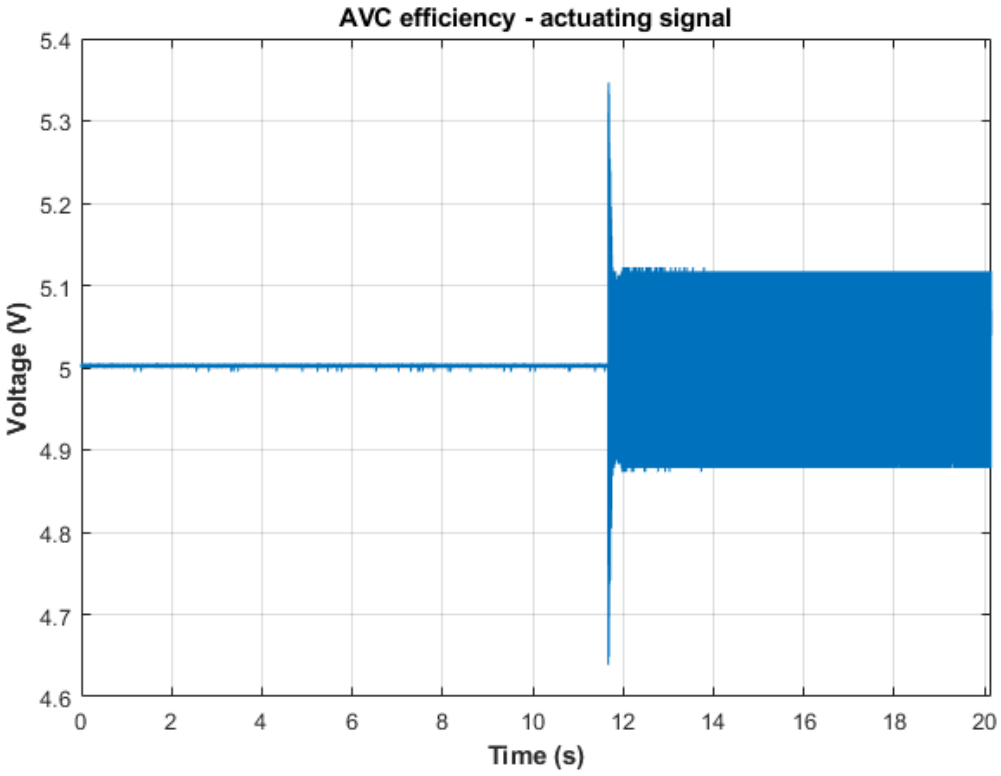

Figure 7.4 Time capture of the actuation signal for first mode when the AVC is switched off

The results of the second mode are shown below.

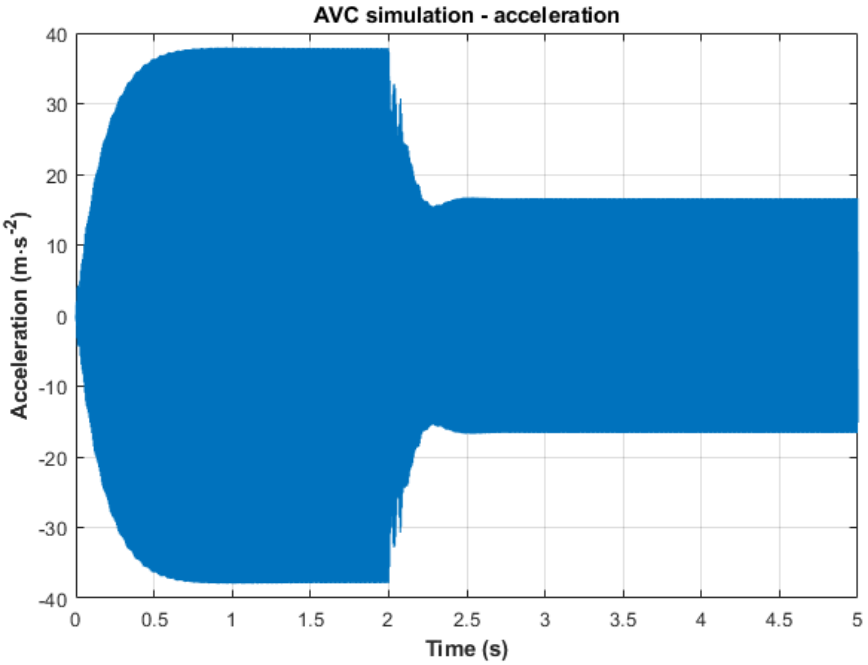

Figure 7.5 Time capture of acceleration for the second mode

The second mode had an excitation frequency of 176.3 Hz and from the graph we can observe the acceleration is 39 m/s^2 before the AVS is turned on and the acceleration reduces to 15 m/s^2. The AVC is turned on after 2 seconds automatically as we use the clock with 2sec timer to turn on the AVC switch.

The Figure 7.6 represents the actuating signal to the piezo and we can see increase in the actuating signal voltage when the AVC is turned on. The actuation signal to the piezo increases as the piezo actuator vibration acts in the opposite way to that of the shaker and provides the control force required to reduce the vibrations.

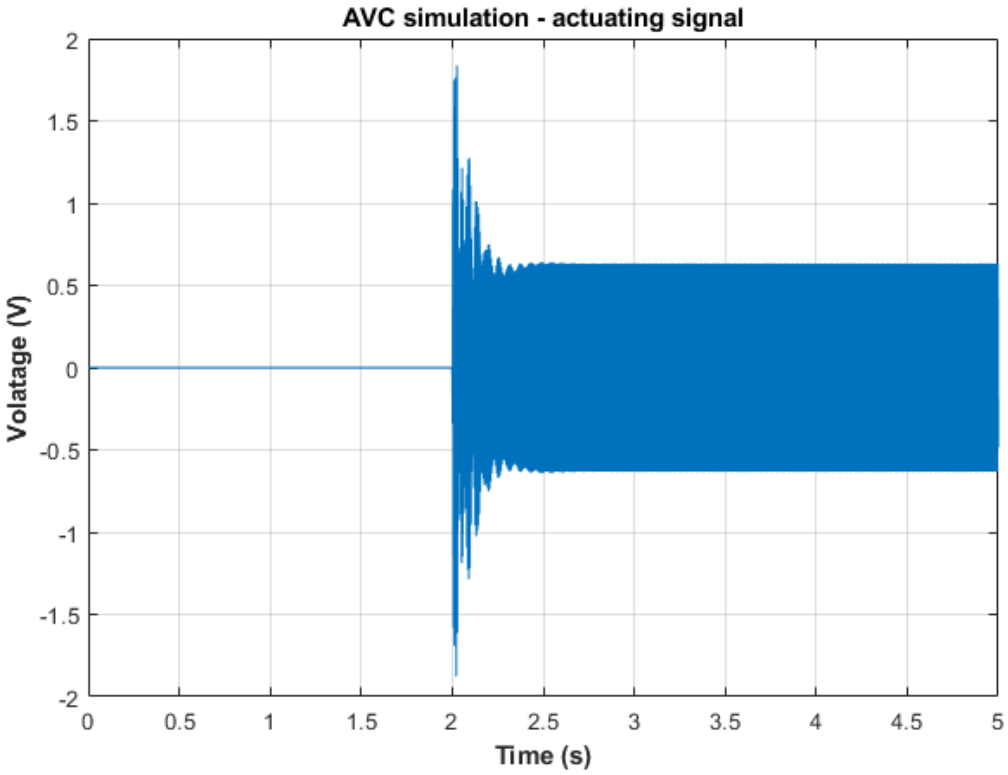

Figure 7.6 Time capture of actuating signal for second mode

The Figure 7.7 in which the blue portion in graph represents when AVC is turned off and the excitation is off and the red portion indication with the excitation to shaker turned on and AVC off and the Green portion represents the AVC turned on and the excitation to the shaker turned on.

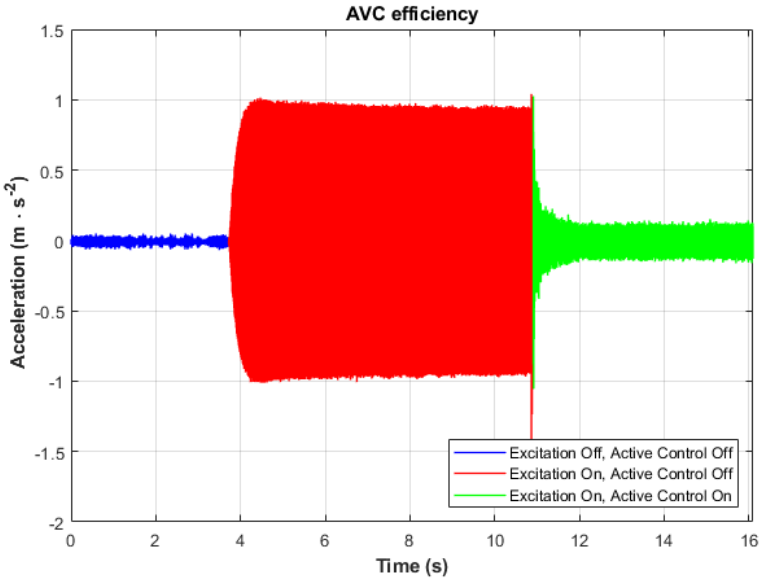

Figure 7.7 Time capture of top mast acceleration for second mode during switching on and off the AVC

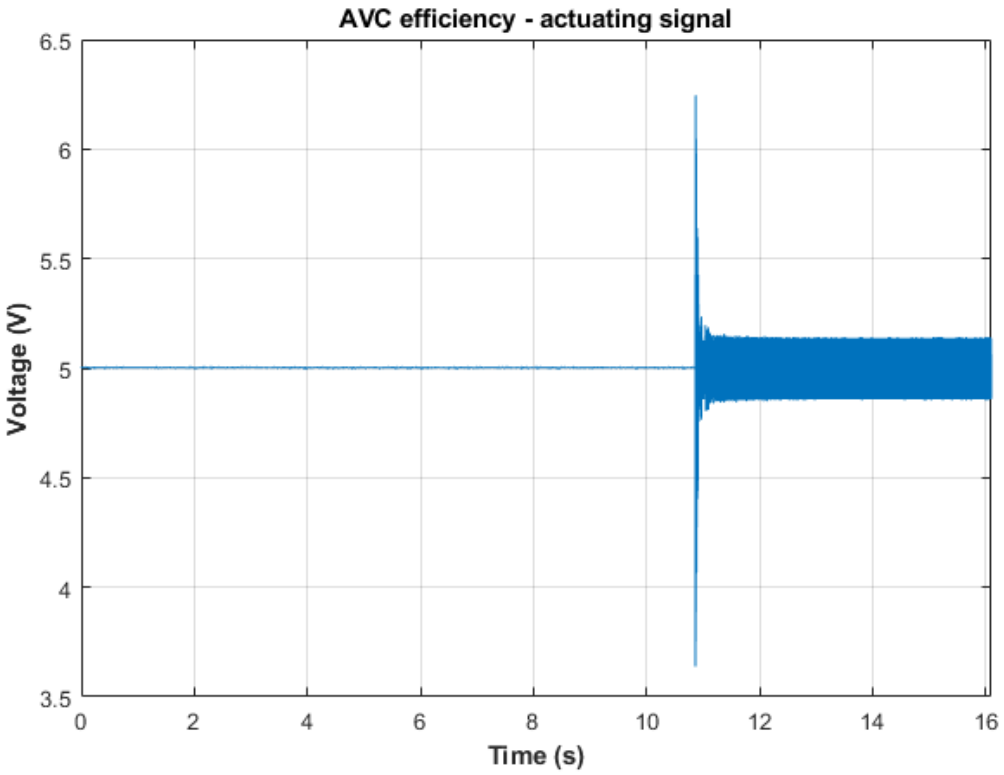

Figure 7.8 Time caption of the actuation signal for second mode when the AVC is switched off

The results of the third mode are shown below.

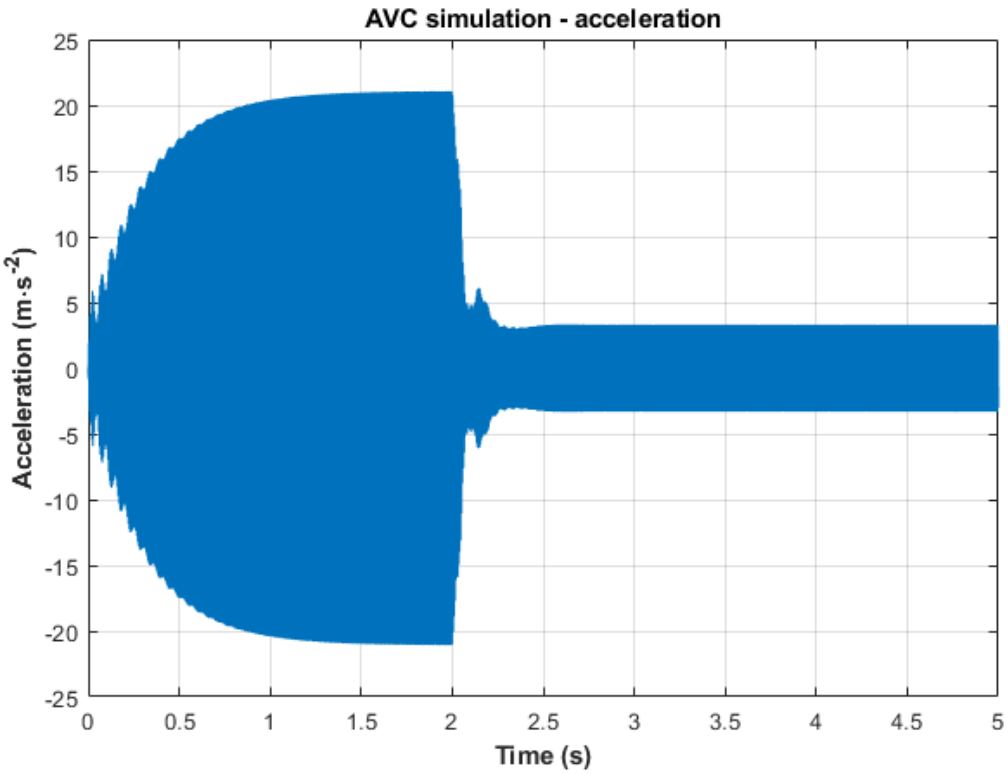

Figure 7.9 Time capture of acceleration for the third mode

The first mode had a excitation frequency of 195 Hz and from the graph we can observe the acceleration is 21 m/s^2 before the AVS is turned on and the acceleration reduces to 4 m/s^2. The AVC is turned on after 2 seconds automatically as we use the clock with 2sec timer to turn on the AVC switch.

The Figure 7.10 represents the actuating signal to the piezo and we can see increase in the actuating signal voltage when the AVC is turned on. The actuation signal to the piezo increases as the piezo actuator vibration acts in the opposite way to that of the shaker and provides the control force required to reduce the vibrations.

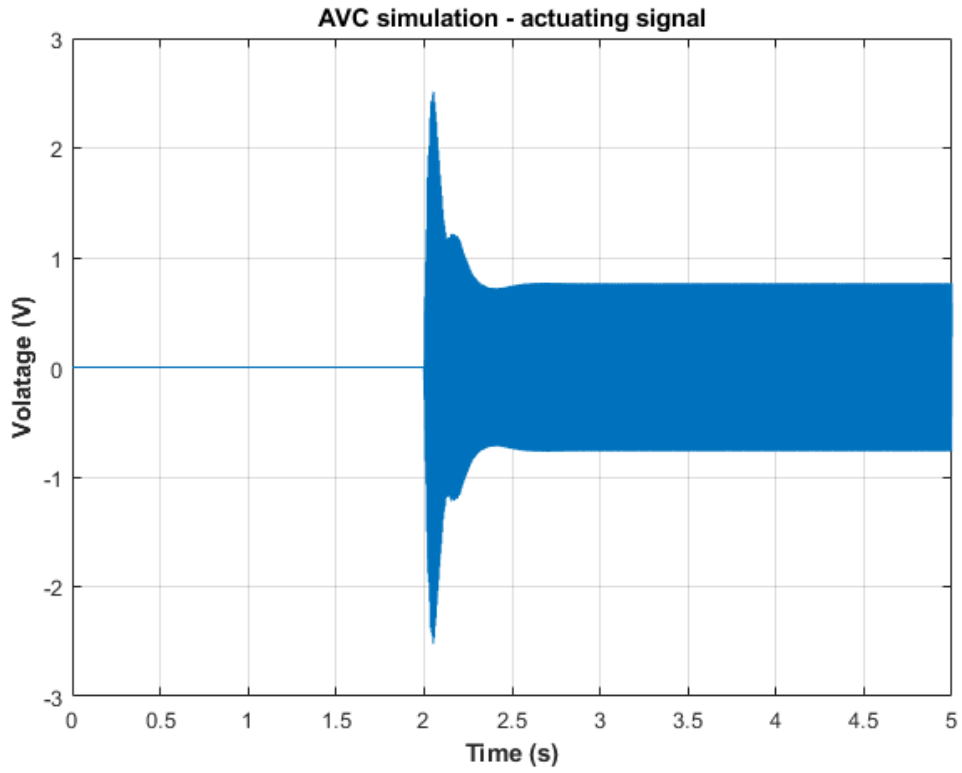

Figure 7.10 Time capture of actuating signal for third mode

The Figure 7.11 in which the blue portion in graph represents when AVC is turned off and the excitation is off and the red portion indication with the excitation to shaker turned on and AVC off and the Green portion represents the AVC turned on and the excitation to the shaker turned on.

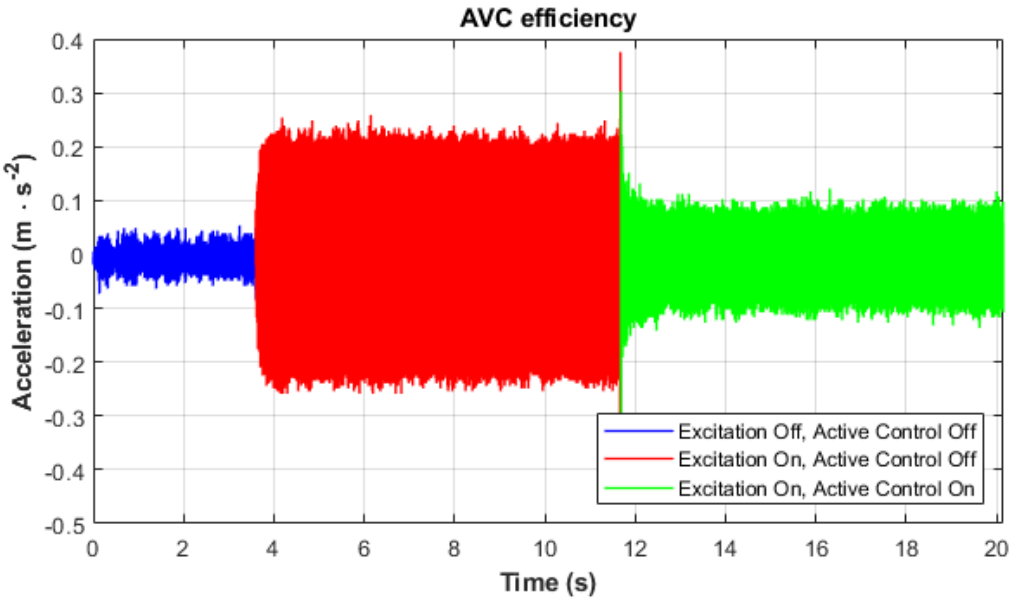

Figure 7.11 Time capture of top mast acceleration for third mode during switching on and off the AVC

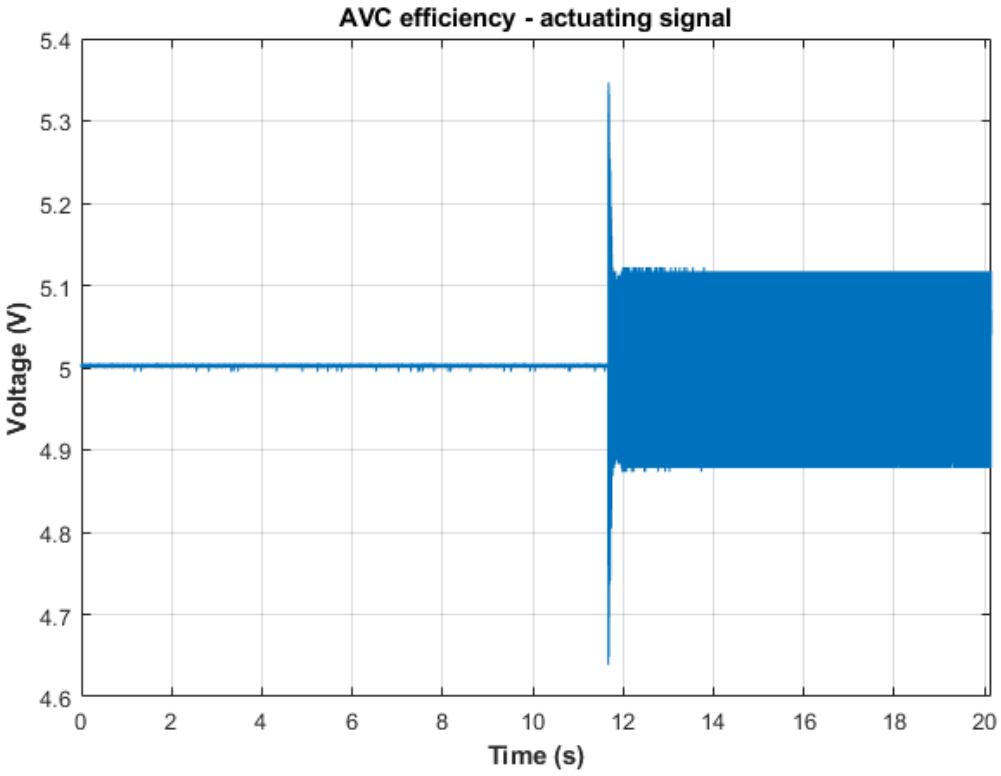

Figure 7.12 Time caption of the actuation signal for third mode when the AVC is switched off

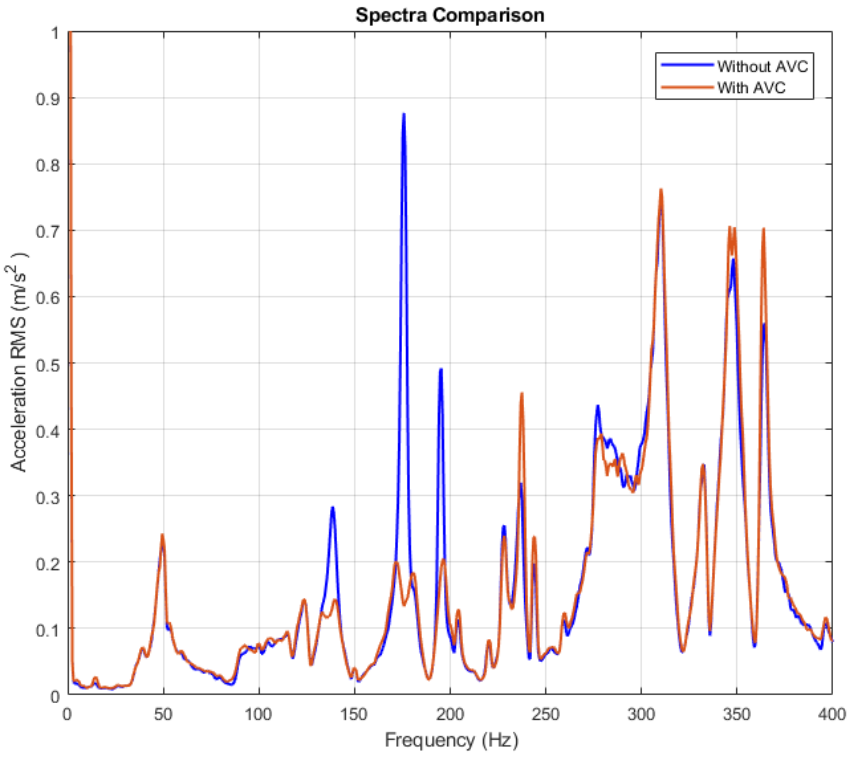

Figure 7.13 Spectra comparison of AVC in frequency domain

The spectra comparison is shown in Figure 7.13 which shows the comparison with and without AVC in frequency domain.

The comparison of the frequency spectrum with AVC turned off is shown using blue line and with AVC turned on is shown is shown using orange line. The excitation was white noise as the input frequency had to have a random seed value to test the effectiveness of the AVC being turned off and on.

As we see the three modes 139.8 Hz, 176.3 Hz and 195 Hz are having acceleration of 0.29 m/s^2, 0.88 m/s^2 and 0.49 m/s^2 when AVC is turned off and they are significantly reduced when the AVC is turned on by 0.15 m/s^2, 0.73 m/s^2 and 0.29 m/s^2 which results in 0.14 m/s^2, 0.15 m/s^2 and 0.2 m/s^2. Hence the effectiveness of the control algorithm designed is proved to be efficient though we see the later parts in the frequency are further amplified as the piezo actuator is not focused to work in that area and the control of these frequencies were not given importance to. The three modes chosen were reduced significantly.

CONCLUSION

In the beginning of the document from the literature survey, I inferred that active vibration structures are vastly used in today's modern world as the natural frequencies of the object is excited due to the weather conditions, loading of additional load and aging of the materials. There are certain situations where when the eyes are exposed to continuous vibrations due to fatigue may lose natural sight (Harazin, 1999). The active vibration control of the structure helps in increasing the efficiency of the working throughout the lifespan required. The active vibration control is spread across wide sectors today in the fields of automobile industry, aeronautical industry, marine industries, logistics and civil engineering. The literature survey was done about the active vibration control and existing methods of active vibration control and the modelling of the structure which is the prototype of the electrical lattice tower was started.

Later the thesis contains details and specifications of project requirement in terms of design after shortlisting from few ideas with changing the connecter block and shape and sizes of the rails and the plate designs. The conclusion was made with the requirements of the design which is described in the beginning of this paper as discussed, the design of individual components used in assembly were designed using Creo parametric design software and the draft of the individual components were made. Then there were adjustments made to the design and final draft was finalised before getting the designed components manufactured as there should be zero errors in this phase of thesis. Hence multiple corrections and checking with the dimensions were done. Then the design was finalised and material for the components were added in the Creo software to get the approximate weight so the overall weight of the assembly could be got to know if the linear rails had sufficient capacity for the weight carrying capacity. The draft copy was sent to the manufacturer and the designed components were manufactured and obtained. Then the assembly of the components designed and procured were assembled into a single assembly. Then the sensors and actuators were attached to the structure and the connection to components such as amplifier and data acquisition module were connected using the cables. Then the measurements for the frequency response function and auto spectrum were done, and the data obtained from the Pulse Labshop were processed in MATLAB software as the conversion was required from matrix form to complex numbers form and the graphs of frequency response function and auto spectrum were plot. The measurements were focused to obtain the frequency response function and auto spectrum. Approximation of frequency response was carried to identify the transfer function of the shaker to accelerometer.

Then the document consists of the control algorithm which was designed using the Simulink tool in MATLAB and then the laboratory model was connected to the instruments and the control algorithm was built in dSpace tool as to build the simulation model to be used to measure and control the laboratory model. Then the measurements were taken, the data was analysed and processed. The efficiency of the active vibration control algorithm was obtained, the effectiveness of the vibration control was seen by the comparison shown in the graph where the vibration without AVC and with using AVC.

The laboratory model for active vibration control was designed and experimental model was assembled. The laboratory model was excited using shaker and piezo separately and the data was acquired using data acquisition module, which was later processed in MATLAB where the identification and approximation was done to obtain the transfer functions. This was followed by design of control algorithm in Simulink where it was tested for active control of vibrations and then the design of control algorithm was executed in dSpace to verify the results experimentally from the excitation to the laboratory model. Then the results were obtained as shown in the results chapter. For the three modes selected which are 139.8 Hz, 176.3 Hz and 195 Hz we observed vibration 0.29 m/s^2, 0.88 m/s^2 and 0.49 m/s^2 when AVC is turned off and they are significantly reduced when the AVC is turned on by 0.15 m/s^2, 0.73 m/s^2 and 0.29 m/s^2 which results in 0.14 m/s^2, 0.15 m/s^2 and 0.2 m/s^2. The respective reduction of vibration in percentage for three modes 139.8 Hz, 176.3 Hz and 195 Hz respectively are 51.72%, 82.95% and 59.18%.

References

Bajkowski, J.M, Dyniewicz, B., Bajer, C.I. 2016. *Semi-active damping strategy for beams system with pneumatically controlled granular structure.* 2016. pp. 387-396. Vol. 70.

Bruel & Kjaer. 2020. Piezoelectric Accelerometer Types 4507 and 4508 (BP-1841). [Online] 04 2020. https://www.bksv.com/en/products/transducers/vibration/accelerometers/4507-B-004.

Damanpack, A., Bodaghi, M., Aghdam, M., Shakeri, M. 2014. *On the vibration control capability of shape memory alloy composite beams.* 2014. pp. 325-334. 110.

Harazin, Barbara. 1999. Study of Effects of Whole-Body Vibration on Visual Auity. *Journal of Low Frequency Noise, Vibration and Active Control.* 1 March 1999, Vol. 18, 1, pp. 13-19.

Kandasamy, Ramkumar, et al. 2016. A review of vibration control methods for marine offshore structures. *Ocean Engineering.* 15 November 2016, Vol. 127, pp. 279-297.

Korkmaz, S. 2011. A review of active structural control: challenges for engineering informatics. Comput. Struct. 89, 2011, Vol. 89, 23, pp. 2113-2132.

Ng, K.W. 1997. Active constrained damping for cylindrical shells. 1997.

Rahman, M., Ong Z.C., Chong, W.T., Julai, S.Khoo, SY. 2015. Renew.Sustain. Energy. 2015, 51, pp. 43-54.

Rao, MD. 2003. Recent applications of viscoelastic damping for noice control in automobile and commercial airplanes. 2003, Vol. 262, 3, pp. 457-474.

Ricciardelli, Pizzimenti, A.D , Mattei, M. 2003. *Passive and active mass damper control of the responce of tall buildings to wind gustiness.* 2003. pp. 1199-1209. Vol. 9.

Takács, Gergely and Rohal'-Ilkiv, Boris. 2012. *Model predictive vibration control: Efficient constrained MPC vibration control for lightly damped mechanical structures.* London : Springer-Verlag, 2012. pp. 1-515. ISBN 978-1-4471-2332-3.

Takács, Gergely, Polóni, Tomáš and Rohal'-Ilkiv, Boris. 2014. Adaptive Model Predictive Vibration Control of a Cantilever Beam with Real-Time Parameter Estimation. *Shock and Vibration.* 7 May 2014, Vol. 2014.

Uppal, S. 1996. Discontineous constrained layer damping treatmets applied to vibrating free beam. 1996.

Vasques, C., Rodrigues, J.D. 2006. *Active vibration control of smart piezoelectric beams:comparison of classical and optimal feedback control strategies.* 2006. pp. 1402-1404. Vol. 22.